Atmos. Chem. Phys. Discuss., 9, 3811–3870, 2009
www.atmos-chem-phys-discuss.net/9/3811/2009/

Atmospheric Chemistry and Physics Discussions

This discussion paper is/has been under review for the journal *Atmospheric Chemistry and Physics (ACP)*. Please refer to the corresponding final paper in *ACP* if available.

Cloud condensation nuclei in pristine tropical rainforest air of Amazonia: size-resolved measurements and modeling of atmospheric aerosol composition and CCN activity

S. S. Gunthe[1], S. M. King[2], D. Rose[1], Q. Chen[2], P. Roldin[3], D. K. Farmer[4], J. L. Jimenez[4], P. Artaxo[5], M. O. Andreae[1], S. T. Martin[2], and U. Pöschl[1]

[1]Max Planck Institute for Chemistry, Biogeochemistry Department, Mainz, Germany
[2]Harvard University, School of Engineering and Applied Sciences & Department of Earth and Planetary Sciences, Cambridge, MA, USA

[3]Lund University, Nuclear Physics, Faculty of Technology, Lund, Sweden
[4]University of Colorado, Dept. of Chemistry & Biochemistry and CIRES, Boulder, CO, USA
[5]Instituto de Fisica, Universidade de Sao Paulo, Sao Paulo, Brazil

Received: 12 December 2008 – Accepted: 19 December 2008 – Published: 4 February 2009

Correspondence to: S. S. Gunthe (gunthe@mpch-mainz.mpg.de)

Published by Copernicus Publications on behalf of the European Geosciences Union.

Abstract

Atmospheric aerosol particles serving as cloud condensation nuclei (CCN) are key elements of the hydrological cycle and climate. We have measured and characterized CCN at water vapor supersaturations in the range of S=0.10–0.82% in pristine tropical rainforest air during the AMAZE-08 campaign in central Amazonia. The effective hygroscopicity parameters describing the influence of chemical composition on the CCN activity of aerosol particles varied in the range of κ=0.05–0.45. The overall median value of $\kappa\approx$0.15 was only half of the value typically observed for continental aerosols in other regions of the world. Aitken mode particles were less hygroscopic than accumulation mode particles ($\kappa\approx$0.1 at $D\approx$50 nm; $\kappa\approx$0.2 at $D\approx$200 nm).

The CCN measurement results were fully consistent with aerosol mass spectrometry (AMS) data, which showed that the organic mass fraction ($X_{m,\mathrm{org}}$) was on average as high as ~90% in the Aitken mode ($D\leq$100 nm) and decreased with increasing particle diameter in the accumulation mode (~80% at $D\approx$200 nm). The κ values exhibited a close linear correlation with $X_{m,\mathrm{org}}$ and extrapolation yielded the following effective hygroscopicity parameters for organic and inorganic particle components: $\kappa_{\mathrm{org}}\approx$0.1 which is consistent with laboratory measurements of secondary organic aerosols and $\kappa_{\mathrm{inorg}}\approx$0.6 which is characteristic for ammonium sulfate and related salts. Both the size-dependence and the temporal variability of effective particle hygroscopicity could be parameterized as a function of AMS-based organic and inorganic mass fractions (κ_p=0.1 $X_{m,\mathrm{org}}$+0.6 $X_{m,\mathrm{inorg}}$), and the CCN number concentrations predicted with κ_p were in fair agreement with the measurement results. The median CCN number concentrations at S=0.1–0.82% ranged from $N_{\mathrm{CCN},0.10}\approx30\,\mathrm{cm}^{-3}$ to $N_{\mathrm{CCN},0.82}\approx150\,\mathrm{cm}^{-3}$, the median concentration of aerosol particles larger than 30 nm was $N_{\mathrm{CN},30}\approx180\,\mathrm{cm}^{-3}$, and the corresponding integral CCN efficiencies were in the range of $N_{\mathrm{CCN},0.10}/N_{\mathrm{CN},30}\approx$0.1 to $N_{\mathrm{CCN},0.82}/N_{\mathrm{CN},30}\approx$0.8.

Although the number concentrations and hygroscopicity parameters were much lower, the integral CCN efficiencies observed in pristine rainforest air were similar to

ACPD
9, 3811–3870, 2009

those in highly polluted mega-city air. Moreover, model calculations of $N_{CCN,S}$ with a global average value of κ=0.3 led to systematic overpredictions, but the relative deviations exceeded ~50% only at low water vapor supersaturation (0.1%) and low particle number concentrations (≤100 cm^{-3}). These findings confirm earlier studies suggesting that aerosol particle number and size are the major predictors for the variability of the CCN concentration in continental boundary layer air, followed by particle composition and hygroscopicity as relatively minor modulators.

Depending on the required and applicable level of detail, the information and parameterizations presented in this paper should enable efficient description of the CCN properties of pristine tropical rainforest aerosols in detailed process models as well as in large-scale atmospheric and climate models.

1 Introduction

Cloud condensation nuclei (CCN) are the subset of atmospheric aerosol particles that enable the condensation of water vapor and formation of cloud droplets at a given level of water vapor supersaturation. They are key elements of the hydrological cycle and climate on regional as well as global scales. Elevated concentrations of CCN tend to increase the concentration and decrease the size of droplets in cloud. Apart from the indirect effect on radiative forcing, this may lead to the suppression of precipitation in shallow and short-lived clouds but also to greater convective overturning and more precipitation in deep convective clouds (Rosenfeld et al., 2008). The response of cloud characteristics and precipitation processes to increasing anthropogenic aerosol concentrations represents one of the largest uncertainties in the current understanding of climate change. One of the crucial challenges is to characterize the hygroscopicity and CCN activity of aerosol particles, i.e., their ability to absorb water vapor and form cloud droplets under relevant atmospheric conditions (e.g. McFiggans et al., 2006; IAPSAG, 2007; IPCC, 2007; Andreae and Rosenfeld, 2008).

During the dry season, the properties and effects of atmospheric aerosols over Ama-

ACPD
9, 3811–3870, 2009

zonia are often strongly influenced by anthropogenic biomass burning emissions (Artaxo et al., 1998, 2002; Andreae et al., 2004; Martin et al., 2009a, and references therein). During the wet season, however, Amazonia is one of the few continental regions on Earth, where the aerosol composition is not dominated by anthropogenic sources and particle properties, interactions and effects can be studied under natural background conditions (Artaxo et al., 1990; Talbot et al., 1990; Andreae, 2007; Martin et al., 2009a, and references therein).

Several studies have investigated the hygroscopicity of Amazonian aerosols by hygroscopicity tandem differential mobility analyzer (HTDMA) experiments, i.e. by the determination of particle growth factors at relative humidities below 100% which can be extrapolated to predict the CCN activity under supersaturated conditions (Zhou et al., 2002; Rissler et al., 2004, 2006; Vestin et al., 2007). Some studies have also applied CCN counters (CCNC) to directly measure CCN concentrations at various levels of water vapor supersaturation (Roberts et al., 2001, 2002, 2003; Andreae et al., 2004; Rissler et al., 2004; Vestin et al., 2007; Freud et al., 2008). Zhou et al. (2002), Rissler et al. (2006), and Vestin et al. (2007) have reported HTDMA and CCNC measurement results from the Amazonian wet season which will be discussed below. So far, however, no size-resolved CCN measurements have been reported from Amazonia.

In the "Amazonian Aerosol Characterization Experiment-2008" (AMAZE-08) campaign during the wet season in February–March 2008 (Martin et al., 2009a), we have used a continuous-flow CCN counter (DMT-CCNC) in combination with an aerosol mass spectrometer (AMS) to characterize the CCN efficiency and chemical composition of pristine tropical rainforest aerosols as a function of dry particle diameter and water vapor supersaturation. To our knowledge such information has not been reported before. In this manuscript we present the measurement data as well as model formalisms and parameters that enable efficient description of the observed CCN properties. Moreover, we compare the results to earlier investigations of the CCN activity of atmospheric aerosol particles in Amazonia and other continental regions.

2 Methods

2.1 Measurement site and meteorological conditions

The measurements were carried out over the period of 14 February to 12 March 2008, i.e. during the Amazonian wet season, at a remote site in the rainforest 60 km of NNW of the city of Manaus in Brazil (2.594541 S, 60.209289 W, 110 m above sea level). The observational tower, (TT34) was located in the Reserva Biologica do Cuieiras and managed by the Instituto Nacional de Pesquisas da Amazonia (INPA) and the Large-Scale Biosphere-Atmosphere Experiment in Amazonia (LBA). As illustrated in Fig. 1, the air masses came mainly from the NE across 1600 km of untouched forest, allowing the study of pristine tropical rainforest conditions. The average meteorological parameters (arithmetic mean ± standard deviation) recorded during the CCN measurement period at the aerosol inlet on top of TT34 were: (297±2) K ambient temperature, (92±10)% ambient relative humidity (RH), (995±5) hPa ambient pressure, (1.2±0.7) m s^{-1} local wind speed, (132±107)° local wind direction. For more information about the measurement location and meteorological conditions see Martin et al. (2009a).

Aerosols from above the forest canopy were sampled through an inlet at the top of TT34 (38.75 m above ground, Rupprecht & Patashnick PM10, ~20 L min^{-1} flow rate) via a stainless steel line (19.05 mm o.d.) to the measurement container at the base of the tower. Before entering the container, the sample flow passed through a diffusion dryer with silica gel/molecular sieve cartridges (alternating regeneration with dry pressurized air, regeneration cycles 15–50 min, average RH=(33±7)%). After drying, the sample flow was split by a manifold and fed into a wide range of aerosol and trace gas measurement instruments. One of the lines led to the CCN measurement setup described below (stainless steel, 6.35 mm o.d., 3 m length, 1.5 L min^{-1} flow rate. For more information about the sampling system and instrumentation of AMAZE-08 see Martin et al. (2009a).

ACPD
9, 3811–3870, 2009

2.2 CCN measurement and data analysis

Size resolved CCN efficiency spectra (CCN activation curves) were measured with a Droplet Measurement Technologies continuous flow CCN counter (DMT-CCNC, Roberts and Nenes, 2005; Lance et al., 2006) coupled to a Differential Mobility Analyzer (DMA; TSI 3071; sheath flow 10 L min^{-1}) and a condensation particle counter (CPC; TSI 3762; sample flow 1.0 L min^{-1} Frank et al., 2006; Rose et al., 2008a). The CCNC was operated at a total flow rate of 0.5 L min^{-1} with a sheath-to-aerosol flow ratio of 10.

The temperature, pressure and relative humidity in the DMA and at the CPC and CCNC inlets were (299±3) K, (995±3) hPa, and (7±6)%, respectively (arithmetic mean ± standard deviation). The CN and CCN concentrations and size distributions reported below refer to these conditions. By multiplication with a factor of 1.10 the concentration values can be normalized to standard temperature and pressure in dry air (273 K, 1000 hPa, 0% RH). The estimated relative uncertainties of the reported CCN measurement results are <20% for individual data points and <10% for the reported average values (Rose et al., 2008a, b).

The effective water vapor supersaturation (S) was regulated by the temperature difference between the upper and lower end of the CCNC flow column (ΔT) and calibrated with ammonium sulfate as described by Rose et al. (2008a, b; Köhler model AP3; calibration line $S=k_s\,\Delta T+S_0$ with k_s=0.0789% K^{-1}, S_0=−0.0909%, R^2=0.9985; relative uncertainty $\Delta S/S$<10%).

For each CCN measurement cycle, ΔT was set to 5 different levels corresponding to S values in the range of 0.10–0.82%. For each ΔT and S, respectively, the diameter of the dry aerosol particles selected by the DMA (D) was set to 9 different values in the range of 20–290 nm depending up on the supersaturation selected. At each D, the number concentration of total aerosol particles (condensation nuclei, CN), N_{CN}, was measured with the CPC, and the number concentration of CCN, N_{CCN}, was measured with the CCNC. The integration time for each measurement data point was

ACPD
9, 3811–3870, 2009

160 s, the recording of a CCN efficiency spectrum (N_{CCN}/N_{CN} vs. D) took ~35 min, and the completion of a full measurement cycle comprising CCN efficiency spectra at 5 different supersaturation levels took ~180 min (including 5 min of settling time for the changeover from highest to lowest S). 169 measurement cycles were performed during the AMAZE-08 campaign from 14 February until 12 March 2008, with occasional short term interruptions for instrument calibration and maintenance and with a four day break due to a power outage and subsequent repair work (2–6 March). Note that for the lowest supersaturation level applied in the atmospheric measurements, the exact mean value S=0.095% was used for the calculations outlined below, but for simplicity a rounded value of 0.10% is listed in figures and tables.

The measurement data points of the CCN efficiency spectra were corrected for the effects of multiply charged particles, differences in the CCNC and CPC counting efficiencies with a constant correction factor f_{corr}=1.05, and the DMA transfer function as described by Rose et al. (2008a, b). For the multiple charge correction we used the total aerosol particle number size distributions that were derived from the CPC measurement data and averaged over each full CCN measurement cycle as described below.

By fitting with cumulative Gaussian distribution functions (CDF), the following parameters were derived from each measured CCN efficiency spectrum (Rose et al., 2008b): the maximum activated fraction MAF_f, the midpoint activation diameter D_a, and the standard deviation σ_a of 3-parameter CDF fits as well as the midpoint activation diameter D_t and the standard deviation σ_t of 2-parameter CDF fits with MAF_f set to 1. Note that the CCN efficiency measured at the largest diameter of each spectrum (MAF_m=N_{CCN}/N_{CN} at D_{max}) was generally in good agreement with MAF_f as derived from the 3-parameter CDF fit.

As detailed by Rose et al. (2008b) the activation diameters and standard deviations derived from the 3-parameter and 2-parameter CDF fits are not the same for CCN efficiency spectra with MAF_f<1: the 3-parameter fit results represent the average properties of the CCN active aerosol particle fraction, whereas the 2-parameter

ACPD
9, 3811–3870, 2009

fit results approximate the overall properties of the external mixture of CCN-active and CCN-inactive particles.

The deviation of MAF_f from unity represents the fraction of externally mixed CCN-inactive particles in the diameter range of D_a to D_{max}. The CDF standard deviations are general indicators for the extent of external mixing and heterogeneity of particle composition in the investigated aerosol: σ_a characterizes the CCN-active particles in the size range around D_a, and σ_t is a measure for the overall heterogeneity of CCN-active and -inactive particles in the size range around D_t. Under ideal conditions, the CDF standard deviations should be zero for an internally mixed, fully monodisperse aerosol with particles of homogenous chemical composition. Even after correcting for the DMA transfer function, however, calibration aerosols composed of high-purity ammonium sulfate exhibit small non-zero σ_a values that correspond to ~3% of D_a and can be attributed to heterogeneities of the water vapor supersaturation profile in the CCNC or other non-idealities such as particle shape effects. Thus, normalized CDF standard deviation or "heterogeneity parameter" values of $\sigma/D \approx 3\%$ indicate internally mixed CCN whereas higher values indicate external mixtures of particles with different chemical composition and hygroscopicity, respectively (Rose et al., 2008b).

For all data pairs of supersaturation and activation diameter derived from the CCN efficiency spectra measured in this study, effective hygroscopicity parameters κ (Petters and Kreidenweis, 2007; Pöschl et al., 2009a) were calculated using the κ-Köhler model equations and parameters specified in Rose et al. (2008b). κ_a calculated from the data pairs of S and D_a characterizes the average hygroscopicity of CCN-active particles in the size range around D_a. κ_t calculated from D_t is an approximate measure (proxy) for the effective hygroscopicity of mixtures of CCN-active and -inactive particles in the size range around D_t (Rose et al., 2008b)

2.3 Determination of CN and CCN size distributions and number concentrations

For each CCN measurement cycle, an average aerosol particle size distribution ($dN_{CN}/d\log D$) was determined from the size-resolved particle number concentrations

ACPD
9, 3811–3870, 2009

measured with the CPC (N_{CN}). Multi-modal lognormal distribution functions were fitted to the measurement data (45 data points of N_{CN} vs. D for 16–27 discrete mobility diameter channels in the range of 20–290 nm selected with the DMA) using the algorithm DO-FIT of Hussein et al. (2005; version 4.20, limited to a maximum of 5 modes). The lognormal fit functions were used to map the measurement data onto a grid of 26 discrete mobility diameter channels with midpoints in the range of D=21.6–819 nm and widths in the range of $d\log D$=0.053–0.079 that were found most suitable for robust data inversion according to Rissler et al. (2006). Upon data inversion, the counting efficiency for the CPC was assumed to be unity for all particles and losses in the sampling lines were neglected. Note that the size distributions displayed in this manuscript extend beyond the upper limit of the measurement range and have to be regarded as extrapolations for D>290. Due to the low concentration of larger particles, however, this has relatively little influence on the reported CN and CCN concentrations and integral CCN efficiencies, respectively.

Aerosol particle (CN) number concentrations were calculated by linear interpolation and stepwise integration of the CN size distributions with a resolution of $d\log D$=0.0083 (Rose et al., 2008b). Besides the integral number concentration for the whole measurement size range starting at 20 nm ($N_{CN,20}$), we have also calculated the concentration of aerosol particles with D>30 nm ($N_{CN,30}$). $N_{CN,30}$ is less influenced by nucleation mode particles (highly variable and generally not CCN-active at S<1%) and by diffusion losses limiting the reliability of the measurement data at D≈20 nm.

The aerosol particle number size distributions obtained by inversion of the CPC measurement data from the DMA-CPC-CCNC system (DMPS) were compared to the results obtained with an SMPS system operated in parallel by Lund University (Roldin et al., 2008), for the period during which both systems were fully operational (~40% of the CCN measurement period), the results were in fair agreement. The SMPS median values were ~20% lower for $N_{CN,20}$, ~5% lower for $N_{CN,30}$, and ~5% lower for the geometric mean diameters of the Aitken and accumulation mode. These differences are likely due to larger diffusion losses or lower counting efficiencies of the SMPS for small

ACPD
9, 3811–3870, 2009

particles.

Averaged over the CCN measurement period, the DMPS values of $N_{CN,20}$ as reported in this paper were ~25% lower than the aerosol particle number concentrations determined with a separate CPC (TSI 3010). To some extent this can be explained by the lower cut-off diameter (~10 nm vs. ~20 nm) and higher time-resolution (1 s vs. 3 h) of the CPC standalone measurements, which are thus more sensitive to nucleation mode particles and short-term events of elevated aerosol concentration. Some deviations may also be due to the DMPS data inversion, diffusive and evaporative losses of small particles in the DMA (lower RH), and potential differences in the CPC flow rates and counting efficiencies. The CPC of the CCN measurement setup (TSI 3762) was calibrated by the manufacturer directly before the campaign, and the deviations from a reference counter were ≤3%.

CCN size distributions ($dN_{CCN}/d\log D$) were calculated by multiplying the CCN efficiency spectra (3-parameter CDF fits of N_{CCN}/N_{CN}) with the total aerosol particle number size distributions derived from the CPC measurement data ($dN_{CN}/d\log D$) and CCN number concentrations ($N_{CCN,S}$) were calculated by stepwise integration of the CCN size distributions (for further details see Rose et al., 2008b).

2.4 Aerosol mass spectrometry (AMS)

An Aerodyne high-resolution time-of-flight aerosol mass spectrometer (HR-ToF-AMS, referred as "AMS" for brevity) was used to measure size-resolved chemical composition of non-refractory submicron aerosol particles (DeCarlo et al., 2006; Canagaratna et al., 2007; Chen et al., 2009). The AMS data used in this study comprise a time series of integral mass concentrations (~5 min time resolution) and a time series of mass size distributions ($dM/d\log d_{va}$, $d\log d_{va}$=0.05, ~6 h time resolution limited by signal-to-noise) where d_{va} is the vacuum aerodynamic diameter (DeCarlo et al., 2004).

To make the size-resolved AMS data directly comparable with the size-resolved CCN data, the AMS d_{va} values were divided by a density scaling factor of 1.4 to obtain approximate mobility equivalent diameters (D) as used throughout this manuscript. The

scaling factor is based on the campaign-average effective particle density of 1.4 g cm^{-3} determined by Chen et al. (2009) from AMS and SMPS measurements according to DeCarlo et al. (2004); it is in good agreement with earlier laboratory and field measurements of organic-rich aerosol particles (Cross et al., 2007; Kostenidou et al., 2007).

For scatter plots and correlations, the non-size-resolved AMS data were averaged over the time intervals of the CCN measurements (~35 min per CCN efficiency spectrum; 1–6 AMS data points per CCN data point). With regard to the size resolved AMS data, the CCN measurement data were averaged over the AMS averaging intervals (~6 h per AMS size distribution; 1-5 CCN data points per AMS data point), and the AMS size distributions were integrated around the midpoint diameters of the CCN efficiency spectra ($D_a \pm \sigma_a$).

3 Results and discussion

3.1 CCN efficiency spectra and related parameters

3.1.1 Campaign averages

From the 30 day campaign period of AMAZE-2008, we have obtained 751 size-resolved CCN efficiency spectra (activation curves) for atmospheric aerosols at five water vapor supersaturations in the range of S=0.10–0.82%. Figure 2 shows campaign averages of the atmospheric CCN efficiency spectra at the different supersaturation levels. The average parameters derived from the CCN efficiency spectra are summarized in Table 1, and their statistical distributions are illustrated in the online supplementary material (http://www.atmos-chem-phys-discuss.net/9/3811/2009/acpd-9-3811-2009-supplement.pdf, Figs. S1–S2). Note that in this paper the terms "entire campaign", "campaign average" and similar expressions generally refer to the period during which the presented size-resolved CCN measurements were performed (14 February–12 March 2008, excluding 2–5 March and some short-term interruptions)

but not to the full duration of the AMAZE-08 campaign (7 February–14 March 2008).

As expected, the midpoint activation diameters D_a increased with S and were larger than the critical diameters for CCN activation of pure ammonium sulfate particles at the given supersaturation levels. In general, the CCN efficiency spectra reached up to one ($MAF_f \approx 1$) and the normalized standard deviations of the 3-parameter CDF fits were small ($\sigma_a/D_a \approx 10\%$), which implies that nearly all aerosol particles larger than the midpoint activation diameter ($D > D_a$) were CCN-active.

At the lowest supersaturation level ($S = 0.10\%$), however, the maximum activated fraction remained on average below one, which indicates the presence of a small fraction of externally mixed CCN-inactive particles with much lower hygroscopicity at $D \approx 200$–250 nm. The average MAF_f was only ~0.9 with minimum values around ~0.7, implying that on average ~10% and up to ~30% of the aerosol particles >200 nm were not CCN-active at $S = 0.10\%$. According to the κ-Köhler model, particles as large as ~250 nm must have an effective hygroscopicity parameter $\kappa < 0.1$ to be not activated at that supersaturation level (Petters and Kreidenweis, 2007; Rose et al., 2008b), indicating substantial proportions of water-insoluble components (e.g. biological materials, black carbon or mineral dust; Petters and Kreidenweis, 2007; Pöschl et al., 2009a).

Figure 3 gives an overview of the effective hygroscopicity parameters (κ_a, κ_t) that have been derived from the midpoint activation diameters (D_a, D_t) of the 3-parameter and 2-parameter CDF fits to the measured CCN efficiency spectra (Sect. 2.2). As detailed by Rose et al. (2009), κ_a characterizes the average hygroscopicity of CCN-active particles in the size range around D_a, whereas κ_t is an approximate measure (proxy) for the effective average hygroscopicity of the total ensemble of aerosol particles in the size range around D_t. On average, κ_t was nearly the same as κ_a. Nevertheless, the small differences observed for large particles (~5% at $D \approx 200$ nm) have a noticeable influence on the calculation of CCN number concentrations at low supersaturation as will be discussed below (Sect. 3.2).

For particles in the Aitken size range (~50–80 nm), the κ values were close to ~0.1, which is characteristic for (secondary) organic aerosol components (King et al., 2007,

ACPD
9, 3811–3870, 2009

2009; Petters and Kreidenweis, 2007; Andreae and Rosenfeld, 2008; Dusek et al., 2009a, b). In the accumulation size range (~100–200 nm), κ increased to ~0.2. Averaged over the full range of aerosol particle sizes and water vapor supersaturations, the median value of the effective hygroscopicity parameter for the Amazonian aerosols investigated during AMAZE-08 was $\kappa \approx 0.15$ (Table 1a). This value is consistent with earlier studies of aerosol particle hygroscopicity during the wet season in Amazonia (Sect. 3.1.3) but only half of the value typically observed for continental aerosols in other regions of the world (Andreae and Rosenfeld, 2008; Rose et al., 2008b).

3.1.2 Time series and focus period

Figure 4 shows time series of characteristic parameters derived from the 3-parameter fits to the CCN efficiency spectra measured throughout the campaign (D_a, κ_a, $\sigma_{a,}/D_a$, MAF_f). For clarity, the parameters in Fig. 4b–d are shown only for the lowest and highest investigated supersaturation levels. The values and temporal evolution of the parameters determined at intermediate supersaturation levels were generally in between those observed at S=0.10% and 0.82%. As for the campaign average values (Table 1), also the time series of the 2-parameter fit results were not much different from the 3-parameter fit results (for time series of D_t, κ_t and $\sigma_{t,}/\mathrm{D}_t$ see online supplement http://www.atmos-chem-phys-discuss.net/9/3811/2009/acpd-9-3811-2009-supplement.pdf, Fig. S3).

Most parameters exhibited considerable short-time variability and some spikes that can be attributed to pollution events and diel cycles related to boundary layer meteorology. In addition to the diel and day-to-day fluctuations, the hygroscopicity parameters observed at S=0.10%, i.e. for accumulation mode particles with diameters around ~200 nm, exhibited a pronounced increase from ~0.15 on 18 February to ~0.3 on 1 March. After a power outage and subsequent repair work on 2–6 March, the κ values were again around ~0.15.

According to AMS data, the variations in κ observed at S=0.1% can be explained by variations in the organic mass fraction of the accumulation mode particles (Sect. 3.3).

The factors regulating the variation in organic mass fraction are not yet fully understood (Chen et al., 2008) but may include local emissions as well as long-range transport of sea salt, mineral dust or biomass burning particles (Martin et al., 2009b). To specifically characterize the CCN properties of aerosol particles in pristine rainforest air, we have chosen a focus period of 6–12 March (start/end 22:00 UTC). During AMAZE-08 this was the longest continuous period with very low aerosol concentrations and high organic mass fractions, which is indicative of minimal influence by long-range transport or local pollution and may thus be most representative of inherent properties of the Amazonian ecosystem (Chen et al., 2008; Martin et al., 2009b). The average CCN parameters for the focus period and for the rest of the campaign are summarized in Table 1, and the statistical distributions are illustrated in the online supplement (Figs. S4–S5, http://www.atmos-chem-phys-discuss.net/9/3811/2009/acpd-9-3811-2009-supplement.pdf).

As shown in Fig. 5, the effective hygroscopicity of accumulation mode particles was substantially lower during the focus period than during the rest of the campaign (~30% at $D \approx 200$ nm), whereas little difference was observed for Aitken mode particles ($D \approx 50$–90 nm). At $S = 0.10\%$ not only κ but also MAF was lower during the focus period (Table 1), indicating a higher proportion of externally mixed CCN-inactive particles at $D \geq 200$ nm. These and other aspects of aerosol composition and mixing state will be discussed below (Sects. 3.3 and 4) and in follow-up studies (Pöschl et al., 2009b).

3.1.3 Comparison with other studies

Earlier studies investigating the CCN activity of aerosol particles in Amazonia during the wet season (Zhou et al., 2002; Rissler et al., 2006; Vestin et al., 2007) did not use the effective hygroscopicity parameter κ but various other parameters to characterize the hygroscopicity of aerosol particles determined by HTDMA measurements: soluble volume fractions referring to an equivalent of ammonium sulfate, ε_{AS}, or ammonium hydrogen sulfate (ammonium bisulfate), ε_{AHS}, or equivalent molar densities of soluble molecules or ions, ρ_{ion} (mol m^{-3}), respectively. For efficient comparison, we have con-

verted these parameters into effective hygroscopicity parameters using the following equation (Petters and Kreidenweis, 2007; Rose et al., 2008a):

$$\kappa \approx \kappa_{AS} \cdot \varepsilon_{AS} \approx \kappa_{AHS} \cdot \varepsilon_{AHS} \approx \rho_{ion}/(\rho_w/M_w) \quad (1)$$

κ_{AS} and κ_{AHS} are the effective hygroscopicity parameters of ammonium sulfate and ammonium hydrogen sulfate, respectively ($\kappa_{AS} \approx \kappa_{AHS} \approx 0.6$); $(\rho_w/M_w) \approx 55 \times 10^3$ mol m^{-3} is the molar density of liquid water (ratio of water density and molar mass). Note that Rissler et al. (2006) and Vestin et al. (2007) had introduced the symbol κ instead of the symbol ρ_{ion}, which was introduced by Wex et al. (2007). In view of the widespread use of the symbol κ for the effective hygroscopicity coefficient as introduced by Petters and Kreidenweis (2007) we took the symbol ρ_{ion} for the equivalent molar density of soluble ions or molecules in the dry particle. The term and subscript "ion" appears not best-suited for the description of water-soluble organic compounds, but we did not want to introduce yet another different symbol at this point.

The exact values of κ, κ_{AS}, κ_{AHS}, ε_{AS}, ε_{AHS} and ρ_{ion} depend on the underlying Köhler model assumptions about the Kelvin and Raoult terms describing the influence of the particle material on the surface tension and water activity of the aqueous droplet formed upon CCN activation (composition- and concentration-dependence of surface tension, osmotic coefficients, van't Hoff factors, etc.; Rose et al., 2008a). Earlier studies have not always unambiguously specified the exact input parameters and formalisms used to determine the reported equivalent soluble volume fractions. In view of other uncertainties related to the experimental calibration and model calculation of water vapor supersaturations, however, the approximation $\kappa \approx 0.6 \cdot \varepsilon_{AS} \approx 0.6 \cdot \varepsilon_{AHS} \approx \rho_{ion}/(55 \times 10^3$ mol m$^{-3})$ should be suitable for comparing HTDMA and CCNC field measurement data from different studies (Rose et al., 2008a; Anderson et al., 2009; Kreidenweis et al., 2008, 2009; Pöschl et al., 2009a).

Table 2 gives an overview of parameters characterizing the externally mixed groups of atmospheric aerosol particles with different hygroscopic properties as observed in the HTDMA measurements of Zhou et al. (2002), Rissler et al. (2006) and Vestin et

ACPD
9, 3811–3870, 2009

al. (2007) during the wet season in Amazonia. These and other HTDMA field measurement studies have used various different designations for the externally mixed groups of particles, including the attributes "hydrophobic" or "nearly hydrophobic", which appear not very well suited to characterize particles that are able to absorb water vapor (albeit not very efficiently). For consistency, we propose and use the following designations: particles with very low hygroscopicity (VLH, κ<0.1), low hygroscopicity (LH, $\kappa\approx$0.1–0.2), medium hygroscopicity (MH, $\kappa\approx$0.2–0.5), or high hygroscopicity (HH, κ>0.5; not relevant in this study).

Zhou et al. (2002), Rissler et al. (2006) and Vestin et al. (2007) reported also CCN concentrations determined with a CCNC, but the CCNC data were not used to derive effective hygroscopicity parameters for the ensemble of aerosol particles that are CCN-active at a given supersaturation (κ_a) or for the overall population of CCN-active and CCN-inactive particles (κ_t). To obtain a proxy for the effective hygroscopicity of the overall population of aerosol particles, we have averaged the κ values of the different groups of particles observed in the HTDMA experiments (VLH, LH, MH; weighted by their number fraction and relative frequency of occurrence), and we have designated this parameter as $\kappa_{t,\mathrm{avg}}$.

As illustrated in Fig. 6, the $\kappa_{t,\mathrm{avg}}$ values derived from the results of Vestin et al. (2007) are very similar to the campaign average κ_t values determined in the present study. They range from ~0.12 for Aitken mode particles to ~0.20 for accumulation mode particles with an overall mean value of ~0.15 (Table 2). The $\kappa_{t,\mathrm{avg}}$ values derived from Zhou et al. (2002) and Rissler et al. (2006) are somewhat lower and similar to the κ_t values determined in the focus period of the present study, ranging from 0.10–0.12 in the Aitken size range to 0.17 in the accumulation size range (overall mean value ~0.13, Table 2).

At the bottom of Table 2 we have summarized the CCNC measurement results of the present study in a format analogous to the presentation of the HTDMA measurement results of earlier studies. The size resolved CCNC measurements do not enable the distinction of externally mixed groups of aerosol particles with different hygroscopicity

(VLH, LH, MH), but they do enable the detection of externally mixed groups of particles that are CCN-active or CCN-inactive at a given supersaturation and size (MAF<1).

Assuming that the CCN-inactive particles observed at S=0.10–0.19% and $D \geq 130$ nm had the same effective hygroscopicity as the VLH particles observed by Vestin et al. (2007; $\kappa \approx 0.074$ at D=165–265 nm), we have calculated $\kappa_{t,\mathrm{avg}}$ values for the mixture of CCN-active and -inactive particles observed by CCNC measurements in the same way as for the mixture of VLH, LH and MH particles observed in HTDMA measurements. For the entire campaign as well as for the focus period (and for the rest of the campaign, not listed), the calculated $\kappa_{t,\mathrm{avg}}$ values are in good agreement with the κ_t values derived from 2-parameter CDF fits to the measured CCN efficiency spectra.

As demonstrated by Rose et al. (2008b) for highly polluted mega-city air and below for pristine rainforest air (Sect. 3.2.2), κ_t is well suited for predicting number concentrations of CCN from atmospheric aerosol size distributions. Thus, the good agreement of $\kappa_{t,\mathrm{avg}}$ and κ_t shown in Table 2 and Fig. 6 indicates that the simple averaging approach taken for the comparison of hygroscopicity parameters derived from HTDMA and CCNC measurements is suitable for (approximately) describing the CCN activity of atmospheric aerosols – at least in Amazonia during the wet season. We suggest that the applicability of κ_t and $\kappa_{t,\mathrm{avg}}$ for efficient comparison and description of the CCN activity of atmospheric aerosol particles should be tested by further investigations combining size-resolved CCNC, HTDMA and particle composition measurements at different locations and conditions (Rose et al., 2009).

Note, however, that the simple averaging approach and effective hygroscopicity parameters/proxies presented above are not meant to replace other more detailed approaches that attempt to resolve externally mixed groups of particles with different hygroscopic properties by more elaborate measurements and models. In fact, more detailed investigations should help to corroborate and/or improve the presented approximations.

Nevertheless, these or similar approximations appear to be not only suitable but also necessary for efficient description of the CCN activity of atmospheric aerosols in studies where only a limited amount of information is available or applicable. Not all measurement instruments, data sets and atmospheric or climate models can provide or process detailed information about aerosol composition and mixing state. Thus, parameters like κ_t and $\kappa_{t,\mathrm{avg}}$ are likely to be useful not only for efficient comparison of different field measurement data sets as in the present study. They may also be useful for studies where only (approximate) aerosol particle concentrations and size distributions are available and applicable, e.g., from satellite remote sensing and long-term monitoring data sets and for long-term climate model calculations.

3.2 CCN size distributions and number concentrations

3.2.1 Measurement results

Figure 7 shows average size distributions of total aerosol particles (CN) and of CCN at different supersaturation levels for the entire campaign, for the focus period, and for the rest of the campaign, respectively. The corresponding median and mean values of integral CN number concentration for the whole measurement range ($N_{\mathrm{CN},20}$) and for particles larger than 30 nm ($N_{\mathrm{CN},30}$), CCN number concentrations ($N_{\mathrm{CCN,S}}$) and CCN efficiencies ($N_{\mathrm{CCN,S}}/N_{\mathrm{CN},20}$, $N_{\mathrm{CCN,S}}/N_{\mathrm{CN},30}$) are summarized in Table 1, and their statistical distributions are illustrated in the online supplementary material (http://www.atmos-chem-phys-discuss.net/9/3811/2009/acpd-9-3811-2009-supplement.pdf, Figs. S6–S7). In the following discussion we focus on $N_{\mathrm{CN},30}$ and $N_{\mathrm{CCN,S}}/N_{\mathrm{CN},30}$ rather than $N_{\mathrm{CN},20}$ and $N_{\mathrm{CCN,S}}/N_{\mathrm{CN},20}$, because the latter are more strongly influenced by nucleation mode particles (highly variable and generally not CCN-active at S<1%) and measurement imprecisions (diffusion losses).

Throughout the campaign, the observed CN number size distributions exhibited pronounced Aitken and accumulation modes around ~70 nm and ~180 nm, respectively. Best-fit parameters of bimodal lognormal size distribution functions fitted to the me-

ACPD
9, 3811–3870, 2009

dian CN size distributions as displayed in Fig. 7 are given in Table 3. The median CN concentrations were similar for the focus period and for the rest of the campaign ($N_{CN,30}$≈180 cm^{-3}), but the relative standard deviations were much higher during the rest of the campaign (~30% vs. ~100%, Table 1), reflecting short-term events with strongly elevated CN concentrations (up to ~2×10^3 cm^{-3}, Fig. 8a).

At low supersaturation (S=0.10%), the median CCN number concentration and integral CCN efficiency ($N_{CCN,S}/N_{CN,30}$) were about three times lower for the focus period (13 cm^{-3}, 0.06) than for the rest of the campaign (39 cm^{-3}, 0.18), which is due to a decrease in size and hygroscopicity of the accumulation mode particles (Fig. 7b vs. 7c). In contrast, the median value of $N_{CCN,S}$ and $N_{CCN,S}/N_{CN,30}$ at high supersaturation (S=0.82%) were higher during the focus period (186 cm^{-3}, 0.78) than during the rest of the campaign (138 cm^{-3}, 0.75), which is mostly due to an increase in the concentration of Aitken mode particles (Fig. 7b vs. 7c).

Figure 8 illustrates the temporal variability of CN and CCN number concentrations with characteristic ranges of ~10^2–10^3 cm^{-3} for $N_{CN,30}$, ~50–300 cm^{-3} for $N_{CCN,0.82}$, and ~5–100 cm^{-3} for $N_{CCN,0.10}$, corresponding to integral CCN efficiencies in the range of ~0.5–0.9 for $N_{CCN,0.82}/N_{CN,30}$ and ~0.05–0.4 for $N_{CCN,0.10}/N_{CN,30}$, respectively.

Averaged over the campaign, the CN and CCN number concentrations observed during AMAZE-08 were up to ~80% lower than those observed in earlier measurements of pristine Amazonian rainforest air, but the integral CCN efficiencies generally agreed to within ~20% (Roberts et al., 2001, 2002; Andreae et al., 2004; Rissler et al., 2004; Vestin et al., 2007). Note that the actual water vapor supersaturation levels in the CCN measurements reported by Roberts et al. (2001, 2002) and Andreae et al. (2004) were ~50% lower than the reported nominal values (Frank et al., 2007)

Compared to highly polluted mega-city regions (Rose et al., 2008b; Wiedensohler et al., 2009), the CN and CCN number concentrations observed during AMAZE-08 were two orders of magnitude lower, but the integral CCN efficiencies were still similar and consistent with the global average values reported by Andreae (2009, $N_{CCN,0.4}/N_{CN,10}$≈0.4).

3.2.2 Approximations and model predictions

In analogy to Rose et al. (2008b) we compare different approaches for the approximation/prediction of CCN concentration as a function of water vapor supersaturation, particle number concentration, size distribution and hygroscopicity: (1) a classical power law approach relating $N_{CCN,S}$ to a constant average value of $N_{CCN,1}$, i.e. to the average CCN concentration at S=1%; (2) a modified power law approach relating $N_{CCN,S}$ to the concentration of aerosol particles with D>30 nm ($N_{CN,30}$); and (3) a κ-Köhler model approach relating $N_{CCN,S}$ to the aerosol particle size distribution ($dN_{CN}/d\log D$) and effective hygroscopicity. For all data points obtained during the campaign, the model predictions were compared with the measurement results, and the mean values of the relative deviations are summarized in Table 4.

Classical power law with constant average $N_{CCN,1}$

Figure 9 shows the median values of $N_{CCN,S}$ plotted against S with power law fits of the form $N_{CCN,S}=N_{CCN,1}(S/1\%)^k$ (Pruppacher and Klett, 1997; OriginPro 8 software, Levenberg-Marquardt algorithm). The best fit values obtained for the CCN number concentration at S=1% (median $N_{CCN,1}$=183 cm^{-3}, mean $N_{CCN,1}$=216 cm^{-3}) are among the lowest values reported from CCN measurements in pristine environments, and the best fit values for the exponent (median k=0.63, mean k=0.70) are in the midst of the range reported for other continental locations (0.4–0.9; Pruppacher and Klett, 1997; Andreae, 2009). The mean relative deviations of the individual measurement data points from the average power laws were in the range of 40–60% for S=0.19–0.82% and as high as ~200% for S=0.10% (Table 5), which is similar to the results obtained by Rose et al. (2008b) for highly polluted air.

Modified power law with variable $N_{CN,30}$

Figure 10 shows the measurement values of $N_{CCN,S}$ plotted against $N_{CN,30}$ and power law fits of the form $N_{CCN,S}=N_{CN,30}\cdot(s)^{-k}$ with $s=1+S/(100\%)$ (OriginPro 8 software, Levenberg-Marquardt algorithm; Pruppacher and Klett, 1997). The best fit values obtained for the exponent q and the corresponding correlation coefficients are listed in Table 5, and the results are similar to those obtained by Rose et al. (2008b). At high supersaturations ($S\geq0.46\%$), $N_{CCN,S}$ was fairly well correlated to $N_{CN,30}$ ($R^2=0.65$–0.90) and the mean relative deviations between the MPL fits and the individual measurement values of $N_{CCN,S}$ were <40%. At low supersaturations ($S\leq0.28\%$) the correlation coefficients were small ($R^2\leq0.5$), but the mean relative deviations were still less than in the CPL approach based on a constant average values of $N_{CCN,1}$.

κ-Köhler model with variable CN size distributions

In Fig. 11 predicted CCN number concentrations ($N_{CCN,S,p}$) that were obtained with the κ-Köhler model and different hygroscopicity parameters are plotted against measurement values of $N_{CCN,S}$. For each data point, $N_{CCN,S,p}$ was calculated by integrating the measured CN size distribution above the critical dry particle diameter for CCN activation that corresponds to the given values of κ and S as detailed in Rose et al. (2008b).

As illustrated in Fig. 11a, the measured and predicted values of $N_{CCN,S}$ are generally in good agreement, when for each data point κ_t is taken from the individual CCN efficiency spectrum measured in parallel to the CN size distribution. With this approach, the mean relative deviation averaged over all supersaturations was only 6%, and the overall mean bias of the model values was +5% (Table 4). The agreement confirms that κ_t is a suitable proxy for the effective hygroscopicity and CCN activity of the investigated ensemble of aerosol particles, including CCN-active and -inactive particles as proposed and demonstrated by Rose et al. (2008b). At $S=0.10$ ($MAF_f\approx0.9$), the mean bias and deviation were highest (+10%, 14%), indicating that the effect of external mixing between CCN-active and -inactive particles is not fully captured by κ_t. Never-

ACPD
9, 3811–3870, 2009

theless, the results obtained with κ_t were clearly better than with κ_a, which represents the effective hygroscopicity of the CCN-active particles only and thus leads to higher mean bias and deviation (+17%, 18%; Table 4). At S=0.19–0.82% where $MAF_f \approx 1$ and $\kappa_a \approx \kappa_t$, the results obtained with individual κ_a values were nearly the same as with individual κ_t, and thus the overall mean bias and deviation were only slightly higher (+6%, 7%; Table 4).

Fair agreement between measured and predicted CCN number concentrations was also achieved when the campaign mean values of $\kappa_t \approx \kappa_a \approx 0.16$ and the corresponding constant activation diameters for the prescribed supersaturation levels ($D_t \approx D_a \approx 200$, 130, 105, 80, and 55 nm) were used for the calculation of $N_{CCN,S,p}$. With these parameters, the mean relative deviations were about twice as high but the bias was only a little higher than when using individual κ_t or κ_a values (Table 4; Fig. 11b).

Figure 11c illustrates the results obtained with composition-based effective hygroscopicity parameters κ_p derived from online aerosol mass spectrometry (AMS) data as detailed below (Sect. 3.3). With these parameters, the mean relative deviations were similar to the ones obtained with the campaign average values of κ_t or κ_a, while the positive bias was somewhat higher (Table 4).

The average effective hygroscopicity parameter observed at other continental locations around the globe, κ=0.3 (Andreae and Rosenfeld, 2008; Rose et al., 2008b; Pöschl et al., 2009a) led to substantial overestimations of $N_{CCN,S}$. The overall mean deviation was ~45%, ranging between ~24% at high S and ~110% at low S (Table 4, Fig. 11d). Note, however, that the bias and deviations of this approach were on average still smaller than with the power law approach based on the campaign average fit values of $N_{CCN,1}$. Time series and statistical distributions of $N_{CCN,S,p}/N_{CCN,S}$ corresponding to the data points of Fig. 11 are shown in the online supplement (http://www.atmos-chem-phys-discuss.net/9/3811/2009/acpd-9-3811-2009-supplement.pdf, Figs. S10–S11).

Clearly, the calculation of CCN number concentrations with κ=0.3 cannot capture the short-term variability and leads to a systematic overprediction in the investigated

tropical rainforest environment with very high proportion of organic particulate matter (Sect. 3.3) and correspondingly low effective hygroscopicity of the aerosol particles. Nevertheless, we consider it remarkable that a constant global average effective hygroscopicity parameter of κ=0.3 (Andreae and Rosenfeld, 2008; Pöschl et al., 2009a) enables the prediction of CCN number concentrations from aerosol particle number size distributions over a range of four orders of magnitude ($N_{CCN,S}$≈10–10^4) going from pristine tropical rainforest air to highly polluted mega-city regions (Rose et al., 2008b) with relative deviations exceeding ~50% only at very low water vapor supersaturations (≤0.1%) and particle number concentrations (≤100 cm^{-3}).

3.3 Aerosol chemical composition and effective hygroscopicity

A detailed presentation and discussion of the AMS measurement results will be given by Chen et al. (2009). Here we only address the relations between AMS and CCN measurement results.

Figure 12 shows the average aerosol mass size distribution of organic compounds and sulfate and the corresponding mass fractions ($X_{m,org}$, $X_{m,SO4}$) as determined by AMS measurements performed in parallel to the CCN measurements. The concentrations and mass fractions of other aerosol constituents measured by the AMS were much smaller (ammonium, nitrate, chloride: $X_{m,NH4}$≈3%, $X_{m,NO3}$≈1%, $X_{m,Cl}$<1%).

In order to make the size-resolved AMS and CCN measurement results directly comparable, Fig. 12 is based on approximate mobility equivalent diameters that have been calculated by division of the AMS vacuum aerodynamic diameter through a density scaling factor of 1.4 (Sect. 2.4; Chen et al., 2009). On the mobility diameter scale, the organic mass size distribution peaks slightly above ~200 nm with a maximum value of ~1.1 $\mu g\,m^{-3}$ per logarithmic decade of particle diameter, while the sulfate size distribution peaks slightly below ~300 nm with a maximum value of only ~0.3 $\mu g\,m^{-3}$. Accordingly, the mass fraction of sulfate increases from ~0.1 at D<100 nm to ~0.3 at D≥200 nm.

This average size dependence of chemical composition is in agreement with the

average size dependence of effective hygroscopicity reported above. As illustrated in Fig. 3, the observed increase of κ with D can be approximately described with the parameterization derived and used below for predicting the temporal variability of κ as a function of $X_{m,\mathrm{org}}$ and $X_{m,\mathrm{SO4}}$ (κ_p=0.1 $X_{m,\mathrm{org}}$+0.6 $X_{m,\mathrm{SO4}}$).

Figure 13 shows the time series of organic and sulfate mass fractions derived from integral AMS measurements, with the organic mass fraction varying mostly in the range of 0.65–0.95. Comparison with Fig. 4b reveals that the highest organic mass fractions, coincided with the lowest κ values observed at S=0.10%, i.e. for accumulation mode particles with D≈200 nm. Especially during the focus period the organic mass fraction was much higher and less variable than during the rest of the campaign (0.91±0.03 vs. 0.76±0.28). On the other hand, elevated sulfate mass fractions, in particular during late February coincided with the highest κ values observed for accumulation mode particles.

In Fig. 14 the effective hygroscopicity parameters derived from the CCN efficiency spectra measured at S=0.10% (κ_a) are plotted against the organic mass fractions ($X_{m,\mathrm{org}}$) determined by integral and size-resolved AMS measurements, respectively. The close correlation between the integral composition data and the size-dependent hygroscopicity parameter (R^2=0.81, Fig. 14a) can be explained by the coincidence of the CCN activation diameter at S=0.10% with the maximum of the aerosol mass size distribution (~200 nm, Fig. 12a). The lower correlation coefficient obtained with the size-resolved AMS data (R^2=0.66, Fig. 14b) is a result of the lower signal-to-noise of these data under the very low concentration conditions of this campaign.

At higher supersaturations corresponding to smaller CCN activation diameters (S=0.19–0.82%, 50–130 nm), neither the integral nor the size-resolved AMS data yielded close correlations between κ_a and $X_{m,\mathrm{org}}$ (R^2<0.5). With regard to the integral AMS data this is due to the size dependence of both κ_a and $X_{m,\mathrm{org}}$ (Figs. 3 and 12b), and with regard to the size-resolved AMS data it can be attributed to low signal-to-noise.

Extrapolation of the fit line in Fig. 14a to $X_{m,\mathrm{org}}$=1 yields an effective hygroscopicity

parameter $\kappa_{org} \approx 0.1$ for the organic fraction of the investigated aerosol particles, which is consistent with laboratory investigations of secondary organic aerosols (Petters and Kreidenweis, 2007; King et al., 2007; Prenni et al., 2007; Engelhart et al., 2008). Under the assumption that the surface tension of the aqueous droplet formed upon CCN activation equals the surface tension of pure water, the effective hygroscopicity parameter κ_{org} can be interpreted as an "effective Raoult parameter", i.e. as an effective molar density of soluble molecules or ions in the dry organic material normalized by the molar density of water molecules in liquid water ($\rho_w/M_w \approx 55\,\mathrm{mol\,L^{-1}}$, Pöschl et al., 2009a):

$$\kappa_{org} \approx i_{org}(\rho_{org}/M_{org})/(\rho_w/M_w) \approx \nu_{org}\Phi_{org}(\rho_{org}/M_{org})/(\rho_w/M_w) \quad (2)$$

To calculate an effective average molecular mass of the organic compounds, M_{org}, we assume that the van't Hoff factor and the product of dissociation number and osmotic coefficient of the organic material, respectively, are close to unity ($i_{org} \approx (\nu\Phi)_{org} \approx 1$) and that the density of the organic material is 1.3–1.4 $\mathrm{g\,cm^{-3}}$ (Cross et al., 2007; King et al., 2007). By inserting these values and $\kappa_{org} \approx 0.10$ into Eq. (2) we obtain an estimate of $M_{org} \approx 230$–$250\,\mathrm{g\,mol^{-1}}$. This is of similar magnitude but somewhat higher than the value of $\sim 180\,\mathrm{g\,mol^{-1}}$ determined for laboratory generated secondary organic aerosol by King et al. (2007) and the value of $\sim 200\,\mathrm{g\,mol^{-1}}$ assumed by Ervens et al. (2007). On the other hand, our estimate of M_{org} for Amazonian aerosols is at the lower end of the range reported for the average molecular mass of water-soluble humic-like substances (HULIS) isolated from atmospheric aerosol samples, which is 215–345 $\mathrm{g\,mol^{-1}}$ according to Kiss et al. (2003) and 250–310 $\mathrm{g\,mol^{-1}}$ according to Salma and Lang (2008), respectively.

Extrapolation of the fit line in Fig. 14a to $X_{m,org} = 0$ yields $\kappa_{inorg} \approx 0.6$ for the inorganic fraction, which is characteristic for ammonium sulfate and related compounds (Petters and Kreidenweis, 2007; Rose et al., 2008a). In fact, the κ values of most compounds typically contributing to the soluble inorganic fraction of continental aerosols are in the range of 0.6 to 0.9 (ammonium bisulfate, ammonium nitrate, sulfuric acid, etc.; Petters

and Kreidenweis, 2007).

By definition, the mixing rule for the κ values of different particle components refers to volume fractions, but mass fractions can be used for first-order approximations (Kreidenweis et al., 2009) assuming that the densities of individual components are similar to the overall particle density, which is reasonable for particles consisting mostly of organics (~1.3–1.4 g cm^{-3}) and sulfate (~1.8 g cm^{-3}; Cross et al., 2007; King et al., 2007; Chen et al., 2009). Thus we have used $\kappa_{org} \approx 0.1$ and $\kappa_{inorg} \approx \kappa_{SO4} \approx 0.6$ to predict effective hygroscopicity parameters from the organic and inorganic mass fractions of determined by AMS ($X_{m,org}$, $X_{m,inorg} = X_{m,SO4} + X_{m,NH4} + X_{m,NO3} \approx X_{m,SO4}$) according to the following equation:

$$\kappa_p = 0.1 \times X_{m,org} + 0.6 \times X_{m,inorg}. \quad (3)$$

Note that this is consistent with the approach that King et al. (2009) have developed and successfully applied to describe the CCN properties of mixed SOA-sulfate particles in laboratory experiments. Moreover, Dusek et al. (2009a) recently found a similar correlation between AMS measurement-based organic and inorganic mass fractions and the effective hygroscopicity of aerosol particles in central Europe.

In Fig. 15 the κ values predicted from the AMS measurement data (κ_p) are plotted against the κ values derived from the 3-parameter fits to the measured CCN efficiency spectra (κ_a). As expected from the above findings, κ_p exhibits a close correlation to κ_a at S=0.10% (R^2=0.77), no close correlation at S=0.19–0.28% (R^2=0.2–0.3), and a pronounced positive bias at S=0.46–0.82% (average offset +0.1, R^2=0.2–0.3). The positive bias of κ_p at high S is due to the enhanced organic mass fraction in small particles and could be corrected on the basis of the average AMS size distribution data (Figs. 3 and 12b), but further processing of the AMS data would go beyond the scope of this study.

In spite of the positive bias and low correlation of predicted vs. measured κ, the mean relative deviations between CCN number concentrations predicted on the basis of κ_p and the measurement values of $N_{CCN,S}$ were mostly less than 20% at S=0.19–

0.82% (Table 4). Although the correlation between κ_p and κ_a was much closer at S=0.10%, the mean relative deviation between $N_{CCN,S,p}$ and $N_{CCN,S}$ was somewhat higher (~27%), which is consistent with the results obtained with the measured κ values. This re-confirms that the prediction of $N_{CCN,S}$ is less robust at low S (Rose et al., 2008b), which is due to the enhanced error-sensitivity caused by the steep slope of the aerosol size distribution typically observed at the large activation diameters corresponding to low supersaturations (Ervens et al., 2007) and also to the stronger influence of externally mixed CCN-inactive particles at large D and low S (Figs. 2–3, Rose et al., 2008b, 2009).

Nevertheless, the AMS-based prediction of $N_{CCN,S}$ at low S worked much better here than in the study of Ervens et al. (2007), who predicted CCN number concentrations based on a combination of particle growth factors measured at subsaturated conditions and AMS data. At low S (~0.07%) they obtained CCN concentrations that were ~2.4 times higher than the measurement values. Note, however, that most likely this was primarily due to problems with the CCN measurement data related to the calibration of the applied CCNC, as hypothesized by Ervens et al. (2007) and confirmed by the results of Rose et al. (2008a). At high supersaturation, Ervens et al. (2007) achieved good agreement between measured and predicted CCN number concentrations.

Overall, the results of the present study confirm that integral AMS measurement data are useful for the prediction of CCN number concentrations from CN size distributions. Highly precise predictions, however, would require size-resolved AMS measurement data of high precision, which are difficult to obtain at the low aerosol concentration levels of pristine tropical rainforest air.

4 Summary and conclusions

4.1 Intensive aerosol and CCN properties

In this paper we presented the first size-resolved CCN measurements in Amazonia. The dry CCN activation diameters measured during AMAZE-08 at S=0.10–0.82% were in the range of 40–240 nm, corresponding to effective hygroscopicity parameters κ in the range of 0.05–0.45. The overall median value of $\kappa \approx 0.15$ is only half of the value typically observed for continental aerosols in other regions of the world, and Aitken mode particles ($D \approx 50$–90 nm, $\kappa \approx 0.1$) were on average less hygroscopic than accumulation mode particles ($D \approx 100$–200 nm, $\kappa \approx 0.2$), which is in good agreement with the results of HTDMA measurements in earlier studies.

The hygroscopicity parameters derived from the CCN measurements are fully consistent with AMS measurement data showing that the organic mass fraction was on average as high as ~90% in the Aitken mode (D<100 nm) and a little lower in the accumulation mode (~80% at $D \approx 200$ nm). The κ values that were determined at low supersaturation, and are most characteristic for the accumulation mode, exhibited a close linear correlation with $X_{m,\mathrm{org}}$. Extrapolation yielded effective average hygroscopicity parameters for the organic and inorganic particle components: $\kappa_{\mathrm{org}} \approx 0.1$ is consistent with laboratory studies of secondary organic aerosol and indicates an effective average molecular mass of ~230–250 g mol^{-1} for the organic compounds; $\kappa_{\mathrm{inorg}} \approx 0.6$ is characteristic for ammonium sulfate and related compounds.

From these results we derived a simple parameterization that approximately describes both the size-dependence and the temporal variability of particle hygroscopicity as a function of AMS-based organic and inorganic mass fractions: $\kappa_p = 0.1 \times X_{m,\mathrm{org}} + 0.6 \times X_{m,\mathrm{inorg}}$. Predicted and measured κ values were in fair agreement, and the mean relative deviation between CCN number concentrations predicted with a κ-Köhler model using κ_p and measured CCN number concentrations was mostly less than 20%.

ACPD
9, 3811–3870, 2009

4.2 Extensive aerosol and CCN properties

The median CCN number concentrations were in the range of $N_{CCN,0.10} \approx 30\,cm^{-3}$ to $N_{CCN,0.82} \approx \sim 150\,cm^{-3}$, and the median concentration of aerosol particles with $D > 30\,nm$ was $N_{CN,30} \approx 180\,cm^{-3}$. The corresponding integral CCN efficiencies were in the range of $N_{CCN,0.10}/N_{CN,30} \approx 0.1$ to $N_{CCN,0.10}/N_{CN,30} \approx 0.8$, which is in good agreement with earlier studies (Roberts et al., 2001, 2002; Andreae et al., 2004; Rissler et al., 2004; Vestin et al., 2007). Although the number concentrations and hygroscopicity parameters were much lower, the average integral CCN efficiencies observed in pristine rainforest air were similar to those reported by Rose et al. (2008) for highly polluted mega-city air and to the global average values reported by Andreae (2009).

Test calculations with different model approaches also confirmed the suitability of κ-Köhler models for the approximation/prediction of CCN number concentrations (Rose et al., 2008). With hygroscopicity parameters derived from CCN or AMS measurement data, the deviation between model and measurement values of $N_{CCN,S}$ was generally less than 10–20%. As expected, the calculation of $N_{CCN,S}$ with a constant global average value of $\kappa = 0.3$ led to overpredictions, but the relative deviations exceeded ~50% only at low water vapor supersaturation (0.1%) and particle number concentrations ($\leq 100\,cm^{-3}$).

4.3 General aspects

The similar integral CCN efficiencies observed in pristine tropical rainforest and in highly polluted mega-cities and the relatively small errors in predicting $N_{CCN,S}$ with constant $\kappa = 0.3$ confirm earlier studies suggesting that aerosol particle number and size are the major predictors for the variability of the CCN concentration in continental boundary layer air, followed by particle composition and hygroscopicity as relatively minor modulators (Dusek et al., 2006; Ervens et al., 2007; Andreae and Rosenfeld, 2008; Rose et al., 2008b; Andreae, 2009; Kreidenweis et al., 2009; Pöschl et al., 2009a). At low S, however, $N_{CCN,S}$ remains difficult to predict with high accuracy. All tested model

ACPD
9, 3811–3870, 2009

approaches yielded mean relative deviations larger than 10% at S=0.1%.

Thus we suggest that future CCN measurements should be focused on low water vapor supersaturation, whereby great care should be taken with regard to instrument calibration (Rose et al., 2008a). In the meantime, the information and parameterizations presented in this and related papers (Table 2) should enable efficient description of the CCN properties of pristine tropical rainforest aerosols in detailed cloud process models as well as in large-scale atmospheric and climate models. Systematic cloud model sensitivity studies should clarify which properties of atmospheric aerosols and CCN activation (number and size, hygroscopicity, mixing state, water uptake kinetics, etc.) are most crucial and should be investigated with priority in order to progress in unraveling aerosol-cloud-climate interactions over Amazonia and around the world.

Acknowledgements. This study was supported by the Max Planck Society (MPG), the European integrated project on aerosol cloud climate and air quality interactions (No 036833-2, EUCAARI), and the Humboldt Foundation (STM Research Fellowship). STM and JLJ acknowledge support received from the U.S. National Science Foundation (ATM-0723582). DKF and JLJ were supported by a NOAA Global Change Postdoctoral Fellowship and NSF grant ATM-0449815. QC acknowledges a NASA Earth and Space Science Fellowship. DKF acknowledges a NOAA Global Change fellowship. Thanks to all AMAZE-08 team members - especially to R. Garland, T. Pauliquevis, F. Morais, P. H. Oliveira, J. Kayse, J. Schneider, S. Zorn, M. Petters and E. Mikhailov – for help, collaboration and exchange during and after the campaign; to A. Wiedensohler and colleagues from IfT Leipzig for preparing the inlet and drying system; to G. Frank and T. Hussein for support in the DMA/CPC data analysis; and to N. Jürgens, D. Pickersgill, J. Schöngart, F. Wittmann, A. Bracho-Nunez, N. Knothe, M. T. Piedade, J. Kesselmeier and the INPA-MPI team for support in the preparation and completion of the campaign. We also thank INPA and the LBA Office in Manaus for logistical support.

This Open Access Publication is financed by the Max Planck Society.

References

Anderson, T. L., Ackerman, A., Hartmann, D. L., Isaac, G. A., Kinne, S., Masunaga, H., Norris, J. R., Pöschl, U., Schmidt, K. S., Slingo, A., and Takayabu, Y. N.: Temporal and Spatial Variability of Clouds and Related Aerosols, in: Clouds in the Perturbed Climate System – Their Relationship to Energy Balance, Atmospheric Dynamics, and Precipitation, edited by: Heintzenberg, J. and Charlson, R. J., MIT Press, Cambridge, 127–147, 2009.

Andreae, M. O.: Aerosols before pollution, Science, 315(5808), 50–51, 2007.

Andreae, M. O.: Correlation between cloud condensation nuclei concentration and aerosol optical thickness in remote and polluted regions, Atmos. Chem. Phys., 9, 543–556, 2009, http://www.atmos-chem-phys.net/9/543/2009/.

Andreae, M. O. and Rosenfeld, D.: Aerosol-cloud-precipitation interactions. Part 1. The nature and sources of cloud-active aerosols, Earth Sci. Rev., 89, 13–41, 2008.

Andreae, M. O., Rosenfeld, D., Artaxo, P., Costa, A. A., Frank, G. P., Longo, K. M., and Silva-Dias, M. A. F.: Smoking rain clouds over the Amazon, Science, 303(5662), 1337–1342, 2004.

Artaxo, P., Fernandes, E. T., Martins, J. V., Yamasoe, M. A., Hobbs, P. V., Maenhaut, W., Longo, K. M., and Castanho, A.: Large-scale aerosol source apportionment in Amazonia, J. Geophys. Res.-Atmos., 103(D24), 31837–31847, 1998.

Artaxo, P., Maenhaut, W., Storms, H., and Vangrieken, R.: Aerosol Characteristics and Sources for the Amazon Basin During the Wet Season, J. Geophys. Res.-Atmos., 95(D10), 16971–16985, 1990.

Artaxo, P., Martins, J. V., Yamasoe, M. A., Procopio, A. S., Pauliquevis, T. M., Andreae, M. O., Guyon, P., Gatti, L. V., and Leal, A. M. C.: Physical and chemical properties of aerosols in the wet and dry seasons in Rondonia, Amazonia, J. Geophys. Res.-Atmos., 107(D20), 8081, doi:10.1029/2001JD000666, 2002.

Canagaratna, M. R., Jayne, J. T., Jimenez, J. L., Allan, J. D., Alfarra, M. R., Zhang, Q., Onasch, T. B., Drewnick, F., Coe, H., Middlebrook, A., Delia, A., Williams, L. R., Trimborn, A. M., Northway, M. J., DeCarlo, P. F., Kolb, C. E., Davidovits, P., and Worsnop, D. R.: Chemical and microphysical characterization of ambient aerosols with the aerodyne aerosol mass spectrometer, Mass Spectr. Rev., 26(2), 185–222, 2007.

Chen, Q., Farmer, D., Allan, J., Borrmann, S., Coe, H., Robinson, N., J., K., Schneider, J., Zom, S., Artaxo, P., Jimenez, J. L., and Martin, S. T.: Characterization of organic

aerosol with a high-resolution time-of-flight aerosol mass spectrometer during the Amazonian Aerosol Characterization Experiment (AMAZE-08), American Association for Aerosol Research, 2008.

Chen, Q., Martin S. T., et al.: manuscript in preparation, 2009.

Cross, E. S., Slowik, J. G., Davidovits, P., Allan, J. D., Worsnop, D. R., Jayne, J. T., Lewis, D. K., Canagaratna, M., and Onasch, T. B.: Laboratory and ambient particle density determinations using light scattering in conjunction with aerosol mass spectrometry, Aerosol Sci. Technol., 41, 343–359, 2007.

DeCarlo, P. F., Kimmel, J. R., Trimborn, A., Northway, M. J., Jayne, J. T., Aiken, A. C., Gonin, M., Fuhrer, K., Horvath, T., Docherty, K. S., Worsnop, D. R., and Jimenez, J. L.: Field-deployable, high-resolution, time-of-flight aerosol mass spectrometer, Analyt. Chem., 78(24), 8281–8289, 2006.

DeCarlo, P. F., Slowik, J. G., Worsnop, D. R., Davidovits, P., and Jimenez, J. L.: Particle morphology and density characterization by combined mobility and aerodynamic diameter measurements. Part 1: Theory, Aerosol Sci. Technol., 38(12), 1185–1205, 2004.

Dusek, U., Frank, G. P., Curtius, J., et al.: CCN activity and composition of aerosol particles during FACE-2005, Geophys. Res. Lett., in preparation, 2009a.

Dusek, U., Stenby, C., Frank, G. P., et al.: CCN activity of laboratory generated SOA particles, Atmos. Chem. Phys. Discuss., in preparation, 2009b.

Dusek, U., Frank, G. P., Hildebrandt, L., Curtius, J., Schneider, J., Walter, S., Chand, D., Drewnick, F., Hings, S., Jung, D., Borrmann, S., and Andreae, M. O.: Size matters more than chemistry for cloud nucleating ability of aerosol particles, Science, 312, 1375–1378, 2006.

Engelhart, G. J., Asa-Awuku, A., Nenes, A., and Pandis, S. N.: CCN activity and droplet growth kinetics of fresh and aged monoterpene secondary organic aerosol, Atmos. Chem. Phys., 8, 3937–3949, 2008, http://www.atmos-chem-phys.net/8/3937/2008/.

Ervens, B., Cubison, M., Andrews, E., Feingold, G., Ogren, J. A., Jimenez, J. L., DeCarlo, P., and Nenes, A.: Prediction of cloud condensation nucleus number concentration using measurements of aerosol size distributions and composition and light scattering enhancement due to humidity, J. Geophys. Res.-Atmos., 112(D10), D10S32, doi:10.1029/2006JD007426, 2007.

Frank, G. P., Dusek, U., and Andreae, M. O.: Technical note: A method for measuring size-

resolved CCN in the atmosphere, Atmos. Chem. Phys. Discuss., 6, 4879–4895, 2006, http://www.atmos-chem-phys-discuss.net/6/4879/2006/.
Freud, E., Rosenfeld, D., Andreae, M. O., Costa, A. A., and Artaxo, P.: Robust relations between CCN and the vertical evolution of cloud drop size distribution in deep convective clouds, Atmos. Chem. Phys., 8, 1661–1675, 2008, http://www.atmos-chem-phys.net/8/1661/2008/.
Hussein, T., Dal Maso, M., Petaja, T., Koponen, I. K., Paatero, P., Aalto, P. P., Hameri, K., and Kulmala, M.: Evaluation of an automatic algorithm for fitting the particle number size distributions, Bor. Environm. Res., 10, 337–355, 2005.
IAPSAG: WMO/IUGG International Aerosol Precipitation Science Assessment Group (IAPSAG) Report: Aerosol Pollution Impact on Precipitation: A Scientific Review. Geneva, World Meteorological Organization, 482, 2007.
IPCC: Climate Change 2007: The Physical Science Basis, Contribution of Working Group I to the Fourth Assessment Report of the Intergovernmental Panel on Climate Change, edited by: Solomon, S., Qin, D., Manning, M., Chen, Z., Marquis, M., Averyt, K., Tignor, M., and Miller, H. L., Cambridge and New York, Cambridge University Press, 996, 2007.
King, S. M., Rosenoern, T., Shilling, J. E., Chen, Q., and Martin, S. T.: Increased cloud activation potential of secondary organic aerosol for atmospheric mass loadings, Atmos. Chem. Phys. Discuss., 9, 1669–1702, 2009, http://www.atmos-chem-phys-discuss.net/9/1669/2009/.
King, S. M., Rosenoern, T., Shilling, J. E., Chen, Q., and Martin, S. T.: Cloud condensation nucleus activity of secondary organic aerosol particles mixed with sulfate, Geophys. Res. Lett., 34(24), L24806, doi:10.1029/2007GL030390, 2007.
Kiss, G., Tombacz, E., Varga, B., Alsberg, T., and Persson, L.: Estimation of the average molecular weight of humic-like substances isolated from fine atmospheric aerosol, Atmos. Environ., 37(27), 3783–3794, 2003.
Kostenidou, E., Pathak, R. K., and Pandis, S. N.: An algorithm for the calculation of secondary organic aerosol density combining AMS and SMPS data, Aerosol Sci. Technol., 41(11), 1002–1010, 2007.
Kreidenweis, S. M., Petters, M. D., and DeMott, P. J.: Single-parameter estimates of aerosol water content, Environ. Res. Lett., 3(3), 035002, doi:10.1088/1748-9326/3/3/035002, 2008.
Kreidenweis, S. M., Petters, M. D., and Chuang, P. Y.: Cloud particle precursors, in: Clouds in the Perturbed Climate System – Their Relationship to Energy Balance, Atmospheric Dy-

namics, and Precipitation, edited by: Heintzenberg, J. and Charlson, R. J., MIT Press, Cambridge, 291–317, 2009.
Lance, S., Medina, J., Smith, J. N., and Nenes, A.: Mapping the Operation of the DMT Continuous Flow CCN Counter, Aerosol Sci. Technol., 40(4), 242–254, 2006.
Martin, S. T., Andreae, M. O., Artaxo, P., Baumgardner, D., Chen, Q., Goldstein, A. H., Guenther, A., Heald, C. L., Mayol-Bracero, O. L., McMurry, P. H., Pauliquevis, T., Pöschl, U., Prather, K. A., Roberts, G. C., Saleska, S. R., Silva-Dias, M. A., Spracklen, D. V., Swietlicki, E., and Trebs, I.: Sources and properties of Amazonian aerosols particles, Rev. Geophys., in review, 2009a.
Martin, S. T., et al.: Amazonian Aerosol Characterization Experiment 2008 (AMAZE-08), Atmos. Chem. Phys. Discuss., in preparation, 2009b.
McFiggans, G., Artaxo, P., Baltensperger, U., Coe, H., Facchini, M. C., Feingold, G., Fuzzi, S., Gysel, M., Laaksonen, A., Lohmann, U., Mentel, T. F., Murphy, D. M., O'Dowd, C. D., Snider, J. R., and Weingartner, E.: The effect of physical and chemical aerosol properties on warm cloud droplet activation, Atmos. Chem. Phys., 6, 2593–2649, 2006, http://www.atmos-chem-phys.net/6/2593/2006/.
Petters, M. D. and Kreidenweis, S. M.: A single parameter representation of hygroscopic growth and cloud condensation nucleus activity, Atmos. Chem. Phys., 7, 1961–1971, 2007, http://www.atmos-chem-phys.net/7/1961/2007/.
Pöschl, U., Rose, D., and Andreae M. O.: Climatologies of Cloud-Related Aerosols – Part 2: Particle Hygroscopicity and Cloud Condensation Nucleus Activity, in: Clouds in the Perturbed Climate System – Their Relationship to Energy Balance, Atmospheric Dynamics, and Precipitation, edited by: Heintzenberg, J. and Charlson, R. J., MIT Press, Cambridge, 58–72, 2009a.
Pöschl, U., Andreae, M. O., Sinha, B., et al.: Amazonian aerosols: bioparticles and organics with a grain of salt, in preparation, 2009b.
Prenni, A. J., Petters, M. D., Kreidenweis, S. M., DeMott, P. J., and Ziemann, P. J.: Cloud droplet activation of secondary organic aerosol, J. Geophy. Res.-Atmos., 112(D10), D10223, doi:10.1029/2006JD007963, 2007.
Pruppacher, H. R. and Klett, J. D.: Microphysics of clouds and precipitation. Dordrecht, Kluwer Academic Publishers, 1997.
Rissler, J., Swietlicki, E., Zhou, J., Roberts, G., Andreae, M. O., Gatti, L. V., and Artaxo, P.: Physical properties of the sub-micrometer aerosol over the Amazon rain forest during the

wet-to-dry season transition - comparison of modeled and measured CCN concentrations, Atmos. Chem. Phys., 4, 2119–2143, 2004, http://www.atmos-chem-phys.net/4/2119/2004/.

Rissler, J., Vestin, A., Swietlicki, E., Fisch, G., Zhou, J., Artaxo, P., and Andreae, M. O.: Size distribution and hygroscopic properties of aerosol particles from dry-season biomass burning in Amazonia, Atmos. Chem. Phys., 6, 471–491, 2006, http://www.atmos-chem-phys.net/6/471/2006/.

Roberts, G. C., Andreae, M. O., Zhou, J., and Artaxo, P.: Cloud condensation nuclei in the Amazon Basin: "marine" conditions over a continent?, Geophys. Res. Lett., 28(14), 2807–2810, 2001.

Roberts, G. C., Artaxo, P., Jingchuan, Z., Swietlicki, E., and Andreae, M. O.: Sensitivity of CCN spectra on chemical and physical properties of aerosol: a case study from the Amazon Basin, J. Geophys. Res., 107(D20), LBA37-1-18, 2002.

Roberts, G. C. and Nenes, A.: A Continuous-Flow Streamwise Thermal-Gradient CCN Chamber for Atmospheric Measurements, Aerosol Sci. Technol., 39(3), 206–221, 2005.

Roberts, G. C., Nenes, A., Seinfeld, J. H., and Andreae, M. O.: Impact of biomass burning on cloud properties in the Amazon Basin, J. Geophys. Res.-Atmos., 108(D2), 4062, doi:10.1029/2001JD000985, 2003.

Roldin, P., Nilsson, E., Swietlicki, E., Massling, A., and Zhou, J.: Lund SMPS User's manual, EUCAARI Brazil version, 2008.

Rose, D., Gunthe, S. S., Mikhailov, E., Frank, G. P., Dusek, U., Andreae, M. O., and Pöschl, U.: Calibration and measurement uncertainties of a continuous-flow cloud condensation nuclei counter (DMT-CCNC): CCN activation of ammonium sulfate and sodium chloride aerosol particles in theory and experiment, Atmos. Chem. Phys., 8, 1153–1179, 2008a, http://www.atmos-chem-phys.net/8/1153/2008/.

Rose, D., Nowak, A., Achtert, P., Wiedensohler, A., Hu, M., Shao, M., Zhang, Y., Andreae, M. O., and Pöschl, U.: Cloud condensation nuclei in polluted air and biomass burning smoke near the mega-city Guangzhou, China – Part 1: Size-resolved measurements and implications for the modeling of aerosol particle hygroscopicity and CCN activity, Atmos. Chem. Phys. Discuss., 8, 17343–17392, 2008b, http://www.atmos-chem-phys-discuss.net/8/17343/2008/.

Rose, D., Garland, R. M., Yang, H., Berghof, M., Wehner, B., Wiedensohler, A., Takegawa, N., Kondo, Y., Andreae, M. O., and Pöschl, U.: Cloud condensation nuclei in polluted air and

biomass burning smoke near the mega-city Guangzhou, China – Part 2: CCN composition and diurnal cycles, Atmos. Chem. Phys. Discuss., in preparation, 2009.

Rosenfeld, D., Lohmann, U., Raga, G. B., O'Dowd, C. D., Kulmala, M., Fuzzi, S., Reissell, A., and Andreae, M. O.: Flood or drought: How do aerosols affect precipitation?, Science, 321(5894), 1309–1313, 2008.

Salma, I. and Láng, G. G.: How many carboxyl groups does an average molecule of humic-like substances contain?, Atmos. Chem. Phys., 8, 5997–6002, 2008, http://www.atmos-chem-phys.net/8/5997/2008/.

Talbot, R. W., Andreae, M. O., Berresheim, H., Artaxo, P., Garstang, M., Harriss, R. C., Beecher, K. M., and Li, S. M.: Aerosol Chemistry During the Wet Season in Central Amazonia – the Influence of Long-Range Transport, J. Geophys. Res.-Atmos., 95(D10), 16955–16969, 1990.

Vestin, A., Rissler, J., Swietlicki, E., Frank, G. P., and Andreae, M. O.: Cloud-nucleating properties of the Amazonian biomass burning aerosol: Cloud condensation nuclei measurements and modeling, J. Geophys. Res.-Atmos., 112(D14), D14201, doi:10.1029/2006JD008104, 2007.

Wex, H., Hennig, T., Salma, I., Ocskay, R., Kiselev, A., Henning, S., Massling, A., Wiedensohler, A., and Stratmann, F.: Hygroscopic growth and measured and modeled critical super-saturations of an atmospheric HULIS sample, Geophys. Res. Lett., 34(2), L02818, doi:10.1029/2006GL028260, 2007.

Wiedensohler, A., Cheng, Y. F., Nowak, A., Wehner, B., Achtert, P., Berghof, M., Birmili, W., Wu, Z. J., Hu, M., Zhu, T., Takegawa, N., Kita, K., Kondo, Y., Lou, S. R., Hofzumahaus, A., Holland, F., Wahner, A., Gunthe, S. S., Rose, D., and Pöschl, U.: Rapid Aerosol Particle Growth and Increase of Cloud Condensation Nucleus (CCN) Activity by Secondary Aerosol Formation: a Case Study for Regional Air Pollution in North Eastern China, J. Geophys. Res.-Atmos., in press, 2009.

Zhou, J. C., Swietlicki, E., Hansson, H. C., and Artaxo, P.: Submicrometer aerosol particle size distribution and hygroscopic growth measured in the Amazon rain forest during the wet season, J. Geophys. Res.-Atmos., 107(D20), 8055, doi:10.1029/2000JD000203, 2002.

Table 1a. Characteristic CCN parameters (median values) averaged over the entire campaign (14 February–12 March 2008), over the pristine focus period (6–12 March, 22:00 UTC), and over the rest of the campaign (14 February–6 March): midpoint activation diameters (D_a,D_t), maximum activated fractions (MAF_f, MAF_m), CDF standard deviations (σ_a, σ_t), heterogeneity parameters (σ_a/D_a, σ_t/D_t), hygroscopicity parameters (κ_a, κ_t), number concentrations of aerosol particles with D>20 nm ($N_{CN,20}$) and with D>30 nm ($N_{CN,30}$), number concentrations of cloud condensation nuclei ($N_{CCN,S}$), integral CCN efficiencies ($N_{CCN,S}/N_{CN,20}$, $N_{CCN,S}/N_{CN,30}$), number of data points (n). Subscripts a and t stand for parameters derived from 3-parameter and 2-parameter CDF fits to the measured CCN efficiency spectra, respectively.

S [%]	D_a [nm]	D_t [nm]	MAF_f	MAF_m	σ_a [nm]	σ_t [nm]	σ_a/D_a	σ_t/D_t	κ_a	κ_t	$N_{CN,30}$ [cm^{-3}]	$N_{CN,20}$ [cm^{-3}]	$N_{CCN,S}$ [cm^{-3}]	$N_{CCN,S}/N_{CN,30}$	$N_{CCN,S}/N_{CN,20}$	n
Entire campaign																
0.10	197.9	200.7	0.92	0.93	8.87	13.02	0.04	0.07	0.196	0.187	187	205	33	0.13	0.11	132
0.19	129.1	130.7	0.98	0.98	9.26	10.95	0.07	0.08	0.184	0.177	182	193	74	0.36	0.30	158
0.28	105.5	105.8	1.00	1.00	7.42	7.29	0.07	0.07	0.154	0.153	176	184	94	0.43	0.37	155
0.46	82.6	83.2	1.01	1.01	6.93	7.28	0.09	0.09	0.114	0.112	181	193	110	0.52	0.46	151
0.82	54.4	55.0	1.00	1.00	3.55	3.98	0.07	0.07	0.120	0.119	174	186	148	0.77	0.69	155
All							0.07	0.08	0.149	0.147	185	198				751
Focus period																
0.10	220.7	224.1	0.88	0.90	7.88	8.92	0.04	0.04	0.143	0.137	197	216	13	0.06	0.06	38
0.19	134.9	135.4	0.99	0.99	6.53	6.33	0.05	0.05	0.164	0.161	195	207	61	0.32	0.30	44
0.28	106.4	106.6	0.99	0.99	5.97	6.21	0.06	0.06	0.150	0.148	197	196	93	0.39	0.37	41
0.46	85.2	86.6	1.01	1.01	5.53	6.38	0.06	0.07	0.105	0.100	196	208	114	0.50	0.46	42
0.82	55.4	55.8	1.01	1.03	2.20	2.10	0.04	0.04	0.118	0.115	184	196	186	0.78	0.73	43
All							0.06	0.06	0.136	0.134	196	202				208
Rest of campaign																
0.10	190.9	192.4	0.92	0.93	9.88	14.39	0.05	0.07	0.215	0.208	187	206	39	0.18	0.15	94
0.19	126.3	128.1	0.98	0.98	11.22	11.82	0.09	0.09	0.193	0.187	178	194	77	0.37	0.31	114
0.28	104.2	104.1	1.00	1.00	8.31	7.86	0.08	0.08	0.161	0.160	175	189	94	0.45	0.38	114
0.46	81.5	82.1	1.00	1.01	7.71	7.57	0.09	0.10	0.117	0.117	177	192	108	0.54	0.46	109
0.82	54.7	54.9	0.99	1.00	4.59	4.97	0.08	0.09	0.122	0.122	168	186	138	0.75	0.67	112
All							0.09	0.09	0.158	0.154	177	192				543

ACPD
9, 3811–3870, 2009

Table 1b. Characteristic CCN parameters (arithmetic mean values ± standard deviations) averaged over the entire campaign (14 February–12 March 2008), over the pristine background (PB) period (6–12 March, 22:00 UTC), and over the rest of the campaign (14 February–6 March): midpoint activation diameters (D_a,D_t), maximum activated fractions (MAF_f, MAF_m), CDF standard deviations (σ_a, σ_t), heterogeneity parameters (σ_a/D_a, σ_t/D_t), hygroscopicity parameters (κ_a, κ_t), number concentrations of aerosol particles with D>20 nm ($N_{CN,20}$) and with D>30 nm ($N_{CN,30}$), number concentrations of cloud condensation nuclei ($N_{CCN,S}$), integral CCN efficiencies ($N_{CCN,S}/N_{CN,20}$, $N_{CCN,S}/N_{CN,30}$), number of data points (n). Subscripts a and t stand for parameters derived from 3-parameter and 2-parameter CDF fits to the measured CCN efficiency spectra, respectively.

S [%]	D_a [nm]	D_t [nm]	MAF_f	MAF_m	σ_a [nm]	σ_t [nm]	σ_a/D_a	σ_t/D_t	κ_a	κ_t	$N_{CN,30}$ [cm^{-3}]	$N_{CN,20}$ [cm^{-3}]	$N_{CCN,S}$ [cm^{-3}]	$N_{CCN,S}/N_{CN,30}$	$N_{CCN,S}/N_{CN,20}$	n
Entire campaign																
0.10	199.0±18.3	201.4±19.6	0.91±0.12	0.93±0.13	11.2±8.8	18.3±18.1	0.06±0.05	0.09±0.09	0.202±0.06	0.195±0.06	237±214	300±276	37±36	0.16±0.12	0.14±0.11	132
0.19	127.9±12.4	129.2±12.6	0.99±0.08	0.99±0.08	10.9±7.7	12.0±9.4	0.09±0.07	0.09±0.07	0.202±0.06	0.196±0.06	221±181	293±289	82±78	0.36±0.13	0.31±0.14	158
0.28	105.3±10.9	105.0±11.3	1.00±0.12	1.00±0.09	9.1±7.1	9.1±6.8	0.09±0.07	0.09±0.06	0.166±0.05	0.164±0.06	221±172	285±277	104±114	0.43±0.13	0.38±0.14	155
0.46	82.8±8.8	83.9±9.2	1.00±0.08	1.01±0.08	8.3±5.9	8.9±6.7	0.10±0.07	0.11±0.08	0.122±0.04	0.118±0.04	224±171	297±291	128±134	0.53±0.13	0.46±0.16	151
0.82	54.6±3.8	54.9±3.9	1.00±0.06	1.00±0.06	4.0±2.7	4.5±3.5	0.07±0.05	0.08±0.07	0.127±0.03	0.124±0.03	215±180	279±275	176±177	0.74±0.11	0.65±0.16	155
All							0.081±0.066	0.092±0.073	0.162±0.061	0.160±0.061	233±203	286±280				751
Pristine focus period																
0.10	217.8±10.0	222.4±12.0	0.91±0.15	0.92±0.16	9.2±8.1	16.3±17.3	0.04±0.04	0.07±0.07	0.149±0.02	0.141±0.02	229±72	255±92	16±10	0.07±0.04	0.06±0.04	38
0.19	132.8±8.1	133.7±7.6	0.99±0.07	0.99±0.07	8.6±5.7	9.4±7.3	0.07±0.05	0.07±0.05	0.175±0.04	0.171±0.03	219±76	243±96	69±29	0.32±0.11	0.30±0.11	44
0.28	108.1±8.1	108.0±8.8	0.98±0.07	0.98±0.07	6.5±3.8	6.7±3.8	0.06±0.03	0.06±0.04	0.147±0.03	0.148±0.04	223±74	238±91	89±31	0.40±0.09	0.38±0.10	41
0.46	86.2±6.6	86.6±6.2	1.00±0.07	1.00±0.07	6.5±4.6	6.5±4.0	0.07±0.05	0.07±0.03	0.103±0.02	0.105±0.02	222±73	249±94	116±40	0.52±0.09	0.47±0.11	42
0.82	55.0±2.2	56.0±2.4	1.00±0.06	1.01±0.06	2.4±1.6	2.7±3.1	0.04±0.03	0.05±0.06	0.121±0.01	0.115±0.02	220±73	245±94	176±64	0.78±0.05	0.72±0.11	43
All							0.06±0.04	0.06±0.05	0.138±0.04	0.137±0.04	221±80	245±86				208
Rest of campaign																
0.10	191.4±15.0	193.3±15.9	0.91±0.11	0.93±0.11	12.0±8.9	19.0±18.5	0.06±0.05	0.10±0.09	0.224±0.06	0.216±0.06	255±261	311±312	45±38	0.20±0.12	0.17±0.11	94
0.19	126.0±13.3	127.5±13.8	0.98±0.08	0.99±0.09	11.8±8.9	13.1±10.0	0.10±0.07	0.10±0.08	0.213±0.07	0.206±0.07	236±221	306±327	88±90	0.37±0.14	0.32±0.15	114
0.28	104.2±11.6	103.9±11.9	1.00±0.14	1.01±0.10	10.0±7.8	10.0±7.4	0.10±0.07	0.10±0.07	0.172±0.06	0.170±0.06	231±207	294±310	110±132	0.44±0.14	0.38±0.16	114
0.46	81.5±9.2	82.8±10.0	1.00±0.08	1.01±0.08	9.0±6.3	9.8±7.3	0.11±0.07	0.12±0.08	0.128±0.04	0.125±0.05	238±208	308±329	133±156	0.53±0.15	0.46±0.17	109
0.82	54.4±4.2	55.5±4.3	0.99±0.06	1.00±0.07	4.7±2.8	5.3±3.4	0.09±0.05	0.10±0.06	0.129±0.03	0.128±0.03	227±220	285±312	176±206	0.73±0.13	0.63±0.17	112
All							0.09±0.07	0.10±0.08	0.171±0.07	0.169±0.07	233±234	301±330				543

ACPD
9, 3811–3870, 2009

Table 2. Parameters characterizing the size-resolved hygroscopicity of aerosol particles in Amazonia during the wet season as observed in earlier studies (HTDMA measurements, campaign average values) and in the present study (CCNC measurements, campaign average and focus period): soluble volume fractions referring to an equivalent of ammonium sulfate (ε_{AS}) or ammonium hydrogen sulfate (ε_{AHS}); equivalent molar densities of soluble molecules or ions (ρ_{ion}); effective hygroscopicity parameters for specific groups and/or size ranges of aerosol particles (κ, κ_a); effective hygroscopicity parameters characterizing the overall aerosol particle population as obtained by averaging over different externally mixed particle groups ($\kappa_{t,avg}=\Sigma_j(\kappa_j \cdot f_{n,j} \cdot f_{o,j})$) or by fitting of measured CCN efficiency spectra (κ_t, 2-parameter CDF fit); number fraction (f_n) and relative frequency of occurrence (f_o) of specific particle groups. The externally mixed particle groups that were detected and differently named in different HTDMA studies are consistently classified according to their hygroscopicity: very low hygroscopicity (VLH, κ<0.1), low hygroscopicity (LH, $\kappa\approx$0.1–0.2), and medium hygroscopicity (MH, $\kappa\approx$0.2–0.5).

Particle group	Parameters							Aitken mode	Accumulation mode	Aitken and accumulation mode	Comments, references
	D (nm)	35	50	75	110	165	265	30–100	100–300	30–300	HTDMA, Sep–Nov 2002,
VLH	ρ_{ion} (mol m^{-3})	4369	4580	4518	4160	3954	4270	4489	4128	4308.5	LBA-SMOCC, Rondônia, Brazil;
	κ	0.079	0.083	0.082	0.075	0.071	0.077	0.081	0.075	0.078	VLH = "nearly hydrophobic particles",
	f_n	0.41	0.48	0.56	0.33	0.19	0.2	0.483	0.24	0.362	LH = "moderately hygroscopic particles";
LH	ρ_{ion} (mol m^{-3})	8396	8378	9401	11 039	10 853	12 463	8725	11 452	10 088	Vestin et al. (2007)
	κ	0.152	0.151	0.170	0.199	0.196	0.225	0.158	0.207	0.182	
	f_n	0.59	0.52	0.44	0.67	0.81	0.8	0.517	0.76	0.638	
All	$\kappa_{t,avg}$	0.122	0.118	0.120	0.158	0.172	0.196	0.120	0.175	0.148	
	D (nm)	35	50	75	110	165	265	30–100	100–300	30–300	HTDMA, Sep-Nov 2002, LBA-SMOCC, Brazil;
VLH	ε_{AS}	0.088	0.09	0.086	0.08	0.091	0.104	0.088	0.092	0.090	VLH = "nearly hydrophobic particles",
	κ	0.053	0.054	0.052	0.048	0.055	0.062	0.053	0.055	0.054	LH = "moderately hygroscopic particles";
	f_n	0.917	0.906	0.769	0.541	0.397	0.343	0.864	0.427	0.6455	Rissler et al. (2006)
	f_o	0.85	0.86	0.95	0.96	0.89	0.92				
LH	ε_{AS}	0.253	0.232	0.254	0.272	0.28	0.32	0.246	0.291	0.2685	
	κ	0.152	0.139	0.152	0.163	0.168	0.192	0.148	0.174	0.161	
	f_n	0.56	0.54	0.45	0.53	0.66	0.69	0.517	0.627	0.572	
	f_o	0.4	0.4	0.6	0.9	0.99	1	0.715	0.963	0.715	
All	$\kappa_{t,avg}$	0.075	0.072	0.079	0.103	0.129	0.152	0.075	0.128	0.102	

Table 2. Continued.

Particle group	Parameters							Aitken mode	Accumulation mode	Aitken and accumulation mode	Comments, references
	D (nm)	35	50	73	109	166	264	30–100	100–300	30–300	HTDMA, Mar–Apr 1998, CLAIRE-98, Balbina, Brazil;
VLH	ε_{AHS}	0.05	0.04	0.03	0.02	0.01	0.02	0.04	0.017	0.028	VLH = "hydrophobic particles",
	κ	0.03	0.024	0.018	0.012	0.006	0.012	0.024	0.01	0.017	LH = "less hygroscopic particles",
	f_n	0.32	0.38	0.45	0.46	0.31	0.24	0.383	0.337	0.360	MH = "more hygroscopic particles";
	f_o	0.06	0.05	0.09	0.13	0.14	0.11	0.067	0.127	0.097	Zhou et al. (2002)
LH	ε_{AS}	0.17	0.15	0.14	0.18	0.21	0.27	0.153	0.22	0.187	
	κ	0.102	0.09	0.084	0.108	0.126	0.162	0.092	0.132	0.112	
	f_n	0.96	0.97	0.96	0.93	0.94	0.97	0.963	0.947	0.955	
	f_o	1	0.95	0.94	0.96	0.95	0.97	0.963	0.960	0.962	
MH	ε_{AHS}	0.6	0.41	0.37	0.4	0.42	0.52	0.46	0.447	0.453	
	κ	0.36	0.246	0.222	0.24	0.252	0.312	0.276	0.268	0.272	
	f_n	0.37	0.68	0.85	0.83	0.82	0.96	0.633	0.870	0.752	
	f_o	0.07	0.09	0.06	0.06	0.07	0.03	0.073	0.053	0.063	
All	$\kappa_{f,avg}$	0.108	0.098	0.088	0.109	0.127	0.162	0.098	0.133	0.115	
	D_a (nm)		54	83	105	129	198	30–100	100–300	30–300	CCNC, AMAZE-08, this study, entire campaign
	D_t (nm)		55	83	105	131	201	30–100	100–300	30–300	
CCN-active	κ_a		0.12	0.114	0.154	0.184	0.196	0.117	0.178	0.1536	
	f_n		1	1	1	0.98	0.92	1	0.97	0.98	
CCN-inactive	κ					0.074	0.074		0.074	0.074	
	f_n					0.02	0.08		0.05	0.05	
All	$\kappa_{f,avg}$		0.120	0.114	0.154	0.182	0.186	0.117	0.174	0.151	
	κ_f		0.119	0.112	0.153	0.177	0.187	0.116	0.172	0.150	
	D_a (nm)		55	85	106	135	221	30–100	100–300	30–300	CCNC, AMAZE-08, this study, focus period
	D_t (nm)		56	87	107	135	224	30–100	100–300	30–300	
CCN-active	κ_a		0.118	0.105	0.15	0.164	0.143	0.112	0.152	0.136	
	f_n		1	1	1	0.99	0.88	1	0.96	0.97	
CCN-inactive	κ					0.074	0.074		0.074	0.074	
	f_n					0.01	0.12		0.06	0.06	
All	$\kappa_{f,avg}$		0.118	0.105	0.150	0.163	0.135	0.112	0.149	0.134	
	κ_f		0.115	0.100	0.148	0.161	0.137	0.108	0.150	0.132	

ACPD
9, 3811–3870, 2009

Table 3. Best-fit parameters of bimodal lognormal size distribution functions fitted to the observed median size distributions of aerosol particles (CN) as displayed in Fig. 7 for the entire campaign, for the focus period, and for the rest of the campaign: integral number concentration (N_{CN}), count median or geometric mean diameter (D_g), and geometric standard deviation (σ_g) for each mode (Aitken and accumulation).

Period	Mode	N_{CN} [cm^{-3}]	D_g [nm]	σ_g
Entire campaign	Aitken	88	57.3	1.49
	Accumulation	86	168	1.43
Focus period	Aitken	82	66.6	1.32
	Accumulation	101	150	1.43
Rest of campaign	Aitken	78	57.7	1.43
	Accumulation	87	173	1.43

ACPD
9, 3811–3870, 2009

Table 4. Characteristic deviations between measured CCN number concentrations ($N_{CCN,S}$) and CCN number concentrations predicted by different model approaches ($N_{CCN,S,p}$): arithmetic mean values of the relative bias ($\Delta_b N_{CCN,S}=(N_{CCN,S,p}-N_{CCN,S})/N_{CCN,S}$) and of the total relative deviation ($\Delta_d N_{CCN,S}=|N_{CCN,S,p}-N_{CCN,S}|/N_{CCN,S}$, including systematic and statistical errors). CPL and MPL are the classical and modified power law approaches. With regard to the κ-Köhler model approach, "κ_a variable", "κ_t variable" and "κ_p variable" stand for the effective hygroscopicity parameters derived from individual CCN efficiency spectra (3- and 2-parameter CDF fits) and from concurrent AMS measurements, respectively; the constant κ values are the campaign medians of κ_t and κ_a and the approximate global average for continental aerosols, respectively. n is the number of data points.

S [%]	CPL		MPL		κ_t variable		κ_a variable		κ_p variable		κ=0.147		κ=0.149		κ=0.3		n
	bias [%]	dev [%]	bias [%]	dev [%]	bias [%]	dev [%]	bias [%]	dev [%]	bias [%]	dev [%]	bias [%]	dev. [%]	bias [%]	dev [%]	bias [%]	dev [%]	
0.10	201.3	220.9	99.5	132.3	10.5	14.3	16.7	18.0	21.2	26.8	−6.4	26.6	−4.3	27.1	110.2	111.3	132
0.19	12.6	51.1	15.0	38.9	3.2	4.1	4.2	4.6	5.0	10.7	−4.4	9.6	−3.8	9.4	24.7	24.9	158
0.28	18.3	52.8	20.6	39.3	4.5	4.9	4.4	5.0	10.7	11.8	3.4	8.8	3.7	8.9	26.5	26.6	155
0.46	24.0	46.8	19.2	35.9	2.1	4.5	3.3	4.2	22.6	22.6	14.0	14.7	14.4	15.1	40.4	40.4	151
0.82	25.5	45.7	15.6	30.6	3.9	4.1	3.4	3.5	14.7	14.8	8.3	8.6	8.7	9.0	24.0	24.0	155
All	56.0	83.3	33.6	55.3	4.63	6.23	6.21	6.89	14.1	16.8	2.8	12.9	3.6	13.7	44.9	45.4	751

ACPD
9, 3811–3870, 2009

Table 5. Best fit parameters for the modified power law (MPL): $N_{CCN,S}=N_{CN,30}\,s^{-q}$. R^2 is the correlation coefficient and n is the number of data points.

S [%]	s	q	R^2	n
0.10	1.001	2031	0.05	132
0.19	1.0019	586	0.32	158
0.28	1.0028	303	0.53	155
0.46	1.0046	135	0.65	151
0.82	1.0082	33	0.90	155

Appendix A

Table A1. Notation (frequently used symbols).

Symbol	Unit	Quantity
D	nm	mobility equivalent dry particle diameter
D_a	nm	midpoint activation diameter determined by 3-parameter CDF fit
D_t	nm	midpoint activation diameter determined by 2-parameter CDF fit
MAF_f		maximum activated fraction determined by 3-parameter CDF fit
$N_{\mathrm{CCN,S}}$	cm^{-3}	CCN number concentration at supersaturation S
$N_{\mathrm{CCN,S,p}}$	cm^{-3}	predicted CCN number concentration at supersaturation S
$N_{\mathrm{CCN,S}}/N_{\mathrm{CN,20}}$, $N_{\mathrm{CCN,S}}/N_{\mathrm{CN,30}}$,	cm^{-3}	integral CCN efficiency relative to N_CN30 and NCN20, respectively
$N_{\mathrm{CN,20}}$, $N_{\mathrm{CN,30}}$	cm^{-3}	CN number concentration of aerosol particles with D>20 nm and with D>30 nm respectively
S	%	water vapor supersaturation
$X_{m,\mathrm{org}}$		organic mass fraction determined by aerosol mass spectrometry
κ		effective hygroscopicity parameter
κ_a		effective hygroscopicity parameter determined by 3-parameter CDF fit (characteristic for CCN-active particles)
κ_p		predicted effective hygroscopicity parameter
κ_t		effective hygroscopicity parameter determined by 2-parameter CDF fit (proxy for overall population of aerosol particles)
$\kappa_{t,\mathrm{avg}}$		effective hygroscopicity parameter determined by averaging over externally mixed particle groups

ACPD
9, 3811–3870, 2009

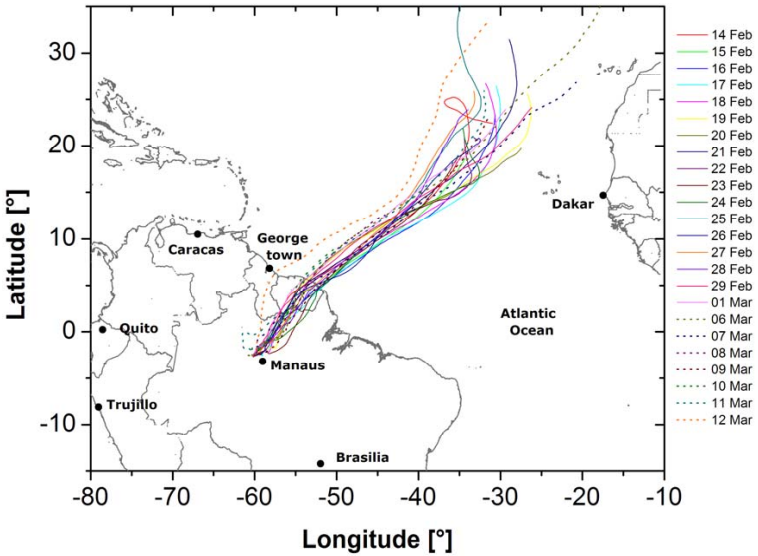

Fig. 1. Location of the AMAZE-08 measurement site in central Amazonia (2.594541 S, 60.209289 W), 60 km NNW of Manaus, Brazil, with 9 day back trajectories (HYSPLIT, NOAA-ARL, GDAS1 model, start height 50 m, start time 23:00 UTC) illustrating the large scale airflow during the CCN measurement period (14 February–12 March 2008). For more information see Martin et al. (2009b).

ACPD
9, 3811–3870, 2009

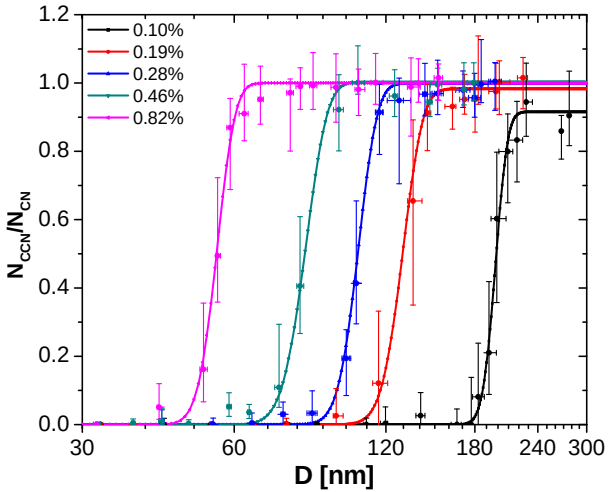

Fig. 2. Size-resolved CCN efficiency spectra at S=0.10–0.82% averaged over the entire campaign: activated particle fraction NCCN/NCN plotted against mobility equivalent diameter D. The data points are median values, the error bars extend from the lower to the upper quartiles, and the lines are 3-parameter cumulative Gaussian distribution function (CDF) fits.

ACPD
9, 3811–3870, 2009

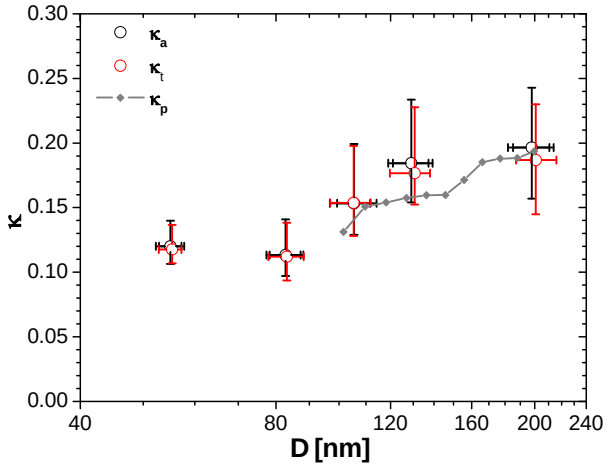

Fig. 3. Effective hygroscopicity parameters (κ_a, κ_t) plotted against the midpoint activation diameters (D_a, D_t) derived from the CCN efficiency spectra (3- and 2-parameter CDF fits) averaged over the entire campaign. The data points are median values corresponding to a given level of supersaturation (S=0.10–0.82%), and the error bars extend to from the lower to the upper quartiles. The gray symbols and line indicate the effective hygroscopicity parameters predicted from the median organic and inorganic mass fractions determined by size-resolved AMS measurements (κ_p).

ACPD
9, 3811–3870, 2009

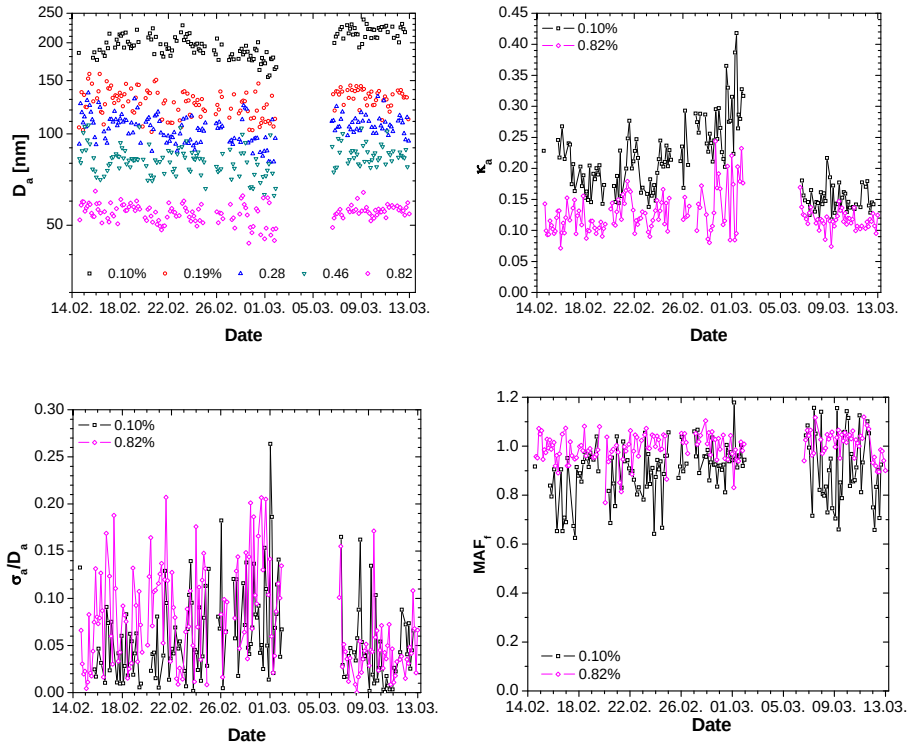

Fig. 4. Time series of characteristic parameters derived from the CCN efficiency spectra (3-parameter CDF fits) observed at different supersaturation levels (S=0.10–0.82%) plotted against the date in February–March 2008 (UTC): midpoint activation diameter (D_a), effective hygroscopicity parameter (κ_a), heterogeneity parameter (σ_a/D_a), and maximum activated fraction (MAF_f).

ACPD
9, 3811–3870, 2009

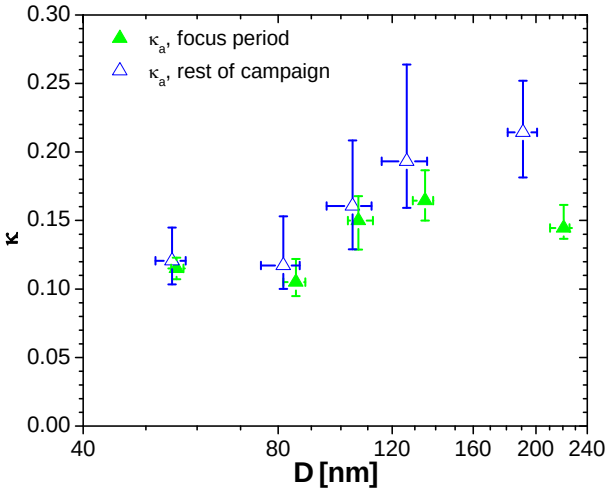

Fig. 5. Effective hygroscopicity parameter of CCN-active particles (κ_a) averaged over the focus period with low aerosol concentrations (6–12 March) and over the rest of the campaign. The data points are median values corresponding to a given level of supersaturation, and the error bars extend to upper and lower quartiles (for equivalent plot with κ_t see online supplement http://www.atmos-chem-phys-discuss.net/9/3811/2009/acpd-9-3811-2009-supplement.pdf, Fig. S9).

ACPD
9, 3811–3870, 2009

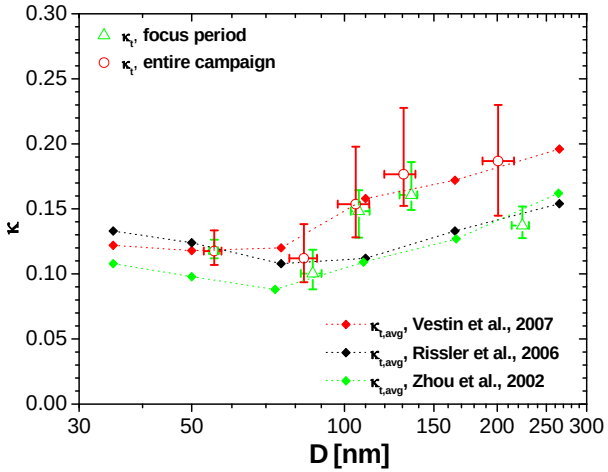

Fig. 6. Effective hygroscopicity parameters for the overall population of aerosol particles observed in pristine Amazonian rainforest air during AMAZE-08 and earlier campaigns during the wet season (CLAIRE 1998, Zhou et al., 2002; LBA-SMOCC 2002, Rissler et al., 2006; Vestin et al., 2007). κ_t was determined by 2-parameter CDF fits to the size-resolved CCN efficiency spectra measured in this study (median values for the entire campaign and for the focus period with error bars extending to upper and lower quartiles). $\kappa_{t,\mathrm{avg}}$ was calculated from the HTDMA measurement results reported by Zhou et al. (2002); Rissler et al. (2006); and Vestin et al. (2007) (campaign average values with connecting lines).

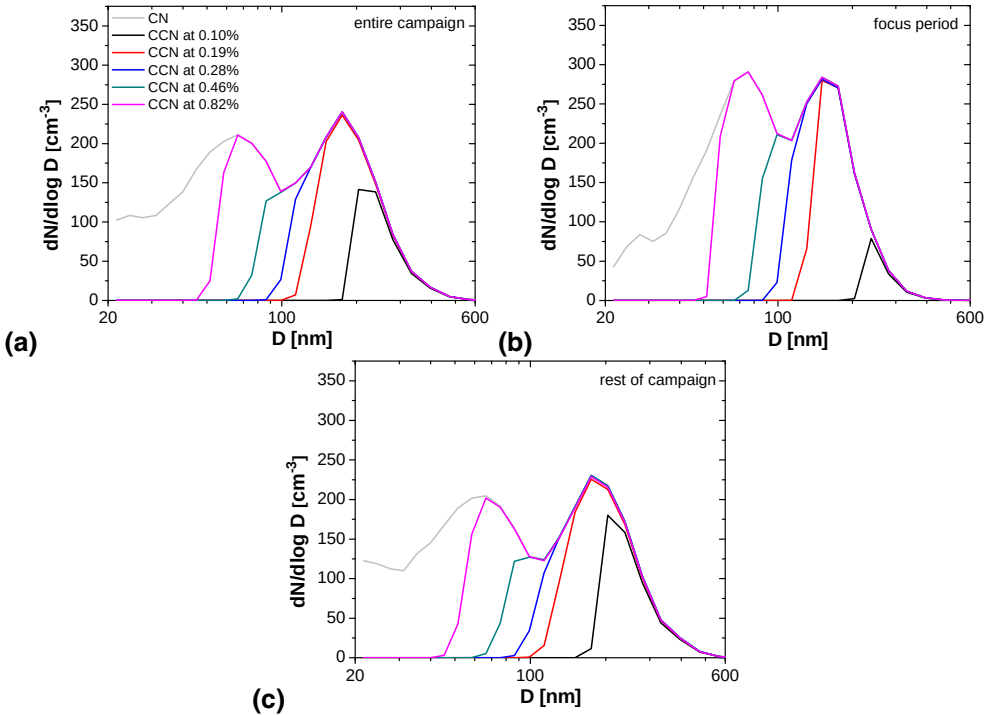

Fig. 7. Number size distributions of total aerosol particles (CN) and of cloud condensation nuclei (CCN) at different supersaturations (S=0.10–0.82%) averaged over the entire campaign **(a)**, over the focus period **(b)**, and over the rest of the campaign **(c)**. The CCN size distributions were calculated by multiplying the median CN size distributions (grey lines) with median CCN efficiency spectra (3-parameter CDF fits).

ACPD
9, 3811–3870, 2009

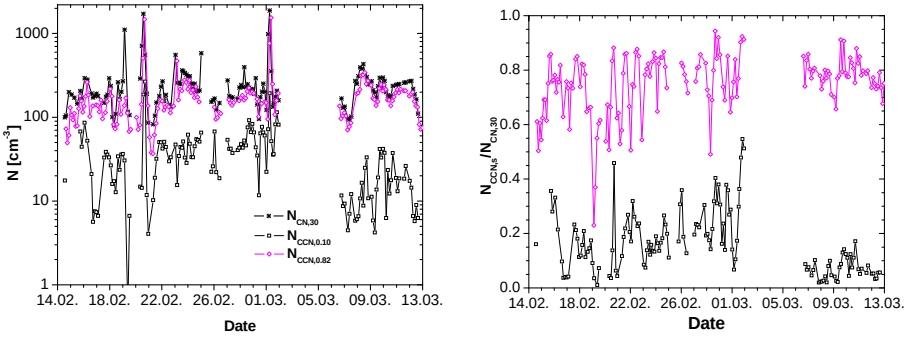

Fig. 8. Time series of the number concentrations of aerosol particles with D>30 nm ($N_{CN,30}$) and cloud condensation nuclei ($N_{CCN,S}$), and of the integral CCN efficiencies ($N_{CCN,S}/N_{CN,30}$) at different supersaturation levels (S=0.10% and 0.82%) plotted against the date in February–March 2008 (UTC). For equivalent plots with $N_{CN,20}$ see online supplement (http://www.atmos-chem-phys-discuss.net/9/3811/2009/acpd-9-3811-2009-supplement.pdf), Fig. S8.

ACPD
9, 3811–3870, 2009

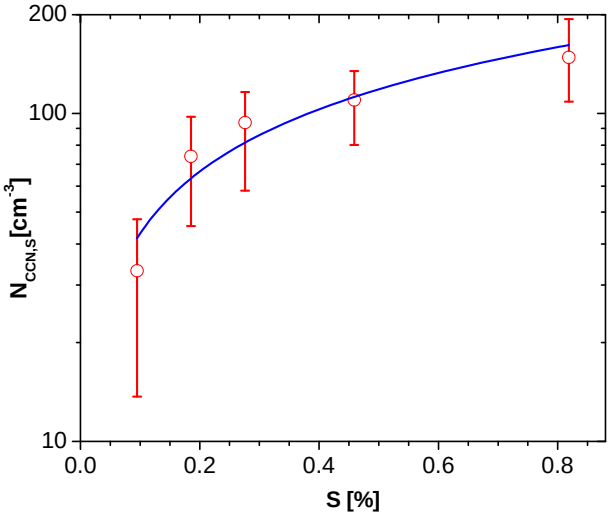

Fig. 9. CCN number concentrations ($N_{CCN,S}$) plotted against water vapor supersaturation (S). The data points are median values, and the error bars extend to lower and upper quartiles for the entire campaign. The blue line is a power law fit of the form $N_{CCN,S}=N_{CCN,1}.(S/(1\%))k$ with the best fit parameters $N_{CCN,1}=183\,cm^{-3}$ and $k=0.63$ ($R^2=0.91$, $n=5$).

ACPD
9, 3811–3870, 2009

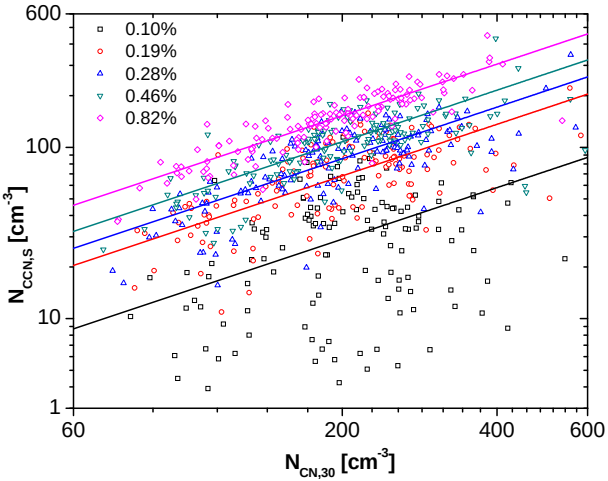

Fig. 10. CCN number concentrations ($N_{CCN,S}$) observed at different supersaturations (S=0.10–0.82%) plotted against the number concentration of aerosol particles with D>30 nm ($N_{CN,30}$). The lines are power law fits of the form $N_{CCN,S}=N_{CN,30}.S^{-q}$; best fit parameters are given in Table 5.

ACPD
9, 3811–3870, 2009

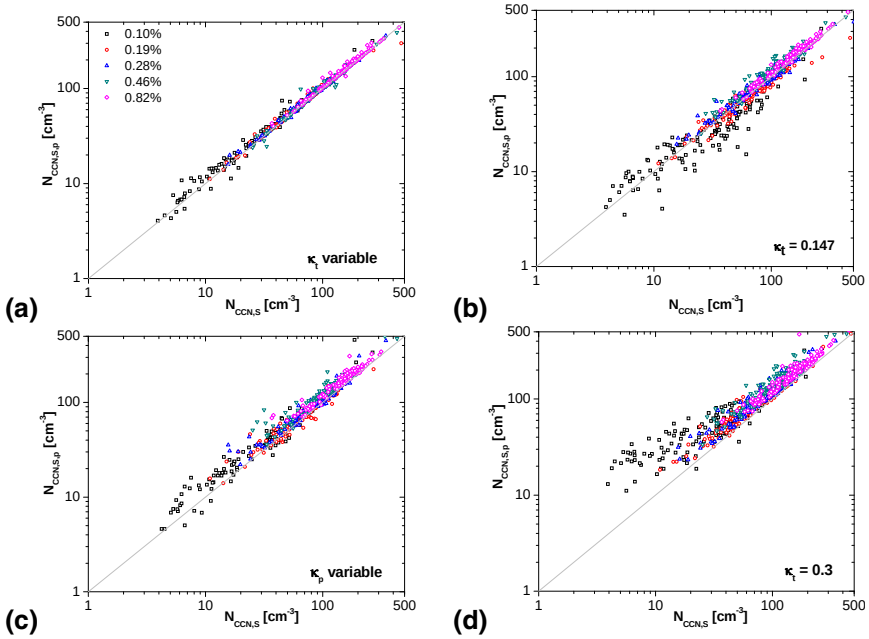

Fig. 11. Predicted vs. measured CCN number concentrations ($N_{CCN,S,p}$ vs. $N_{CCN,S}$). Predictions are based on the κ-Köhler model approach using different types of effective hygroscopicity parameters: **(a)** with variable values of κ_t as derived from the individual CCN efficiency spectra; **(b)** with a constant average value of κ_t=0.147; **(c)** with variable values of κ_p predicted from the organic and sulfate mass fractions determined by AMS; and **(d)** with a constant global average value of κ_t=0.3.

ACPD
9, 3811–3870, 2009

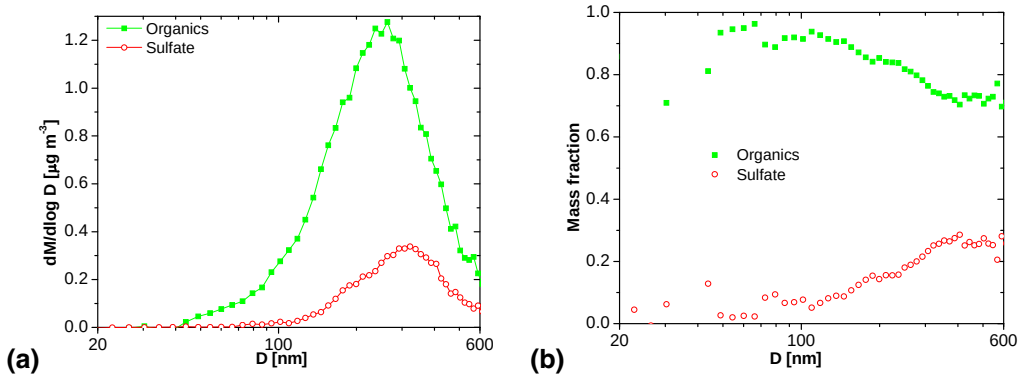

Fig. 12. Mass size distribution **(a)** and corresponding mass fractions **(b)** of organics and sulfate determined by aerosol mass spectrometry (AMS) averaged over the CCN measurement period. The diameter values (D) are approximate mobility equivalent diameters calculated by division of the AMS vacuum aerodynamic diameter through 1.4 (dimensionless density scaling factor).

ACPD
9, 3811–3870, 2009

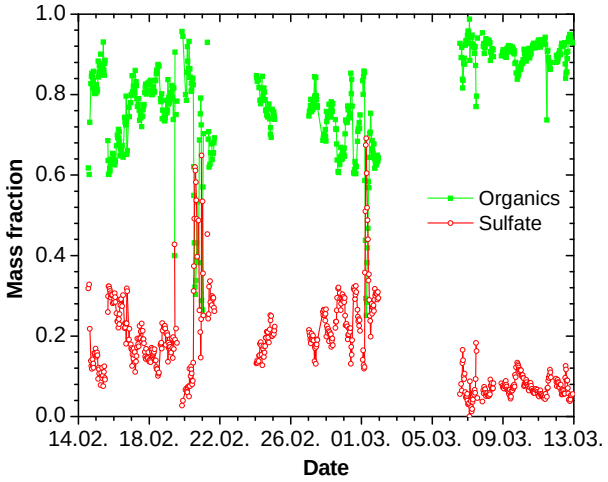

Fig. 13. Time series of organic and sulfate mass fractions determined by integral AMS measurements, averaged over the CCN measurement intervals, and plotted against the date in February–March 2008 (UTC).

ACPD
9, 3811–3870, 2009

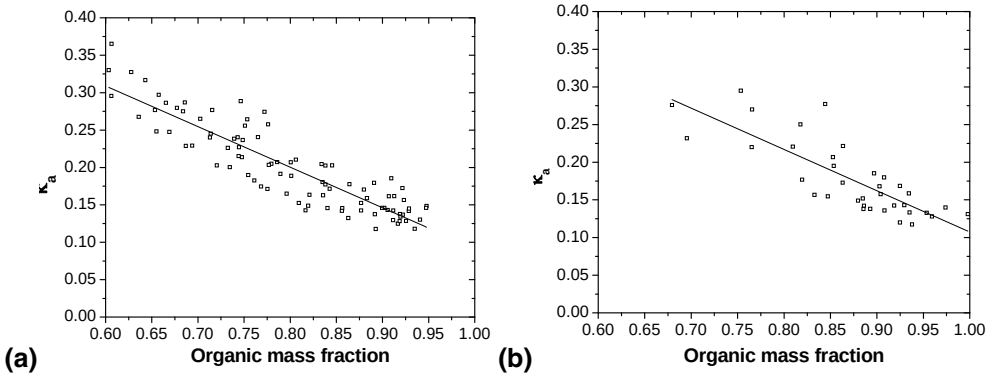

Fig. 14. Correlations between the effective hygroscopicity of CCN (κ_a) observed at S=0.1% and the organic mass fraction ($X_{m,\mathrm{org}}$) determined by **(a)** integral and **(b)** size-resolved AMS measurements. Linear fit equations, correlation coefficients, and numbers of data points: (a) y=0.634–0.543x, R^2=0.81, n=97; (b) y=0.656–0.548x, R^2=0.66, n=36 (for equivalent plots with κ_t see online supplement (http://www.atmos-chem-phys-discuss.net/9/3811/2009/acpd-9-3811-2009-supplement.pdf, Fig. S12).

ACPD
9, 3811–3870, 2009

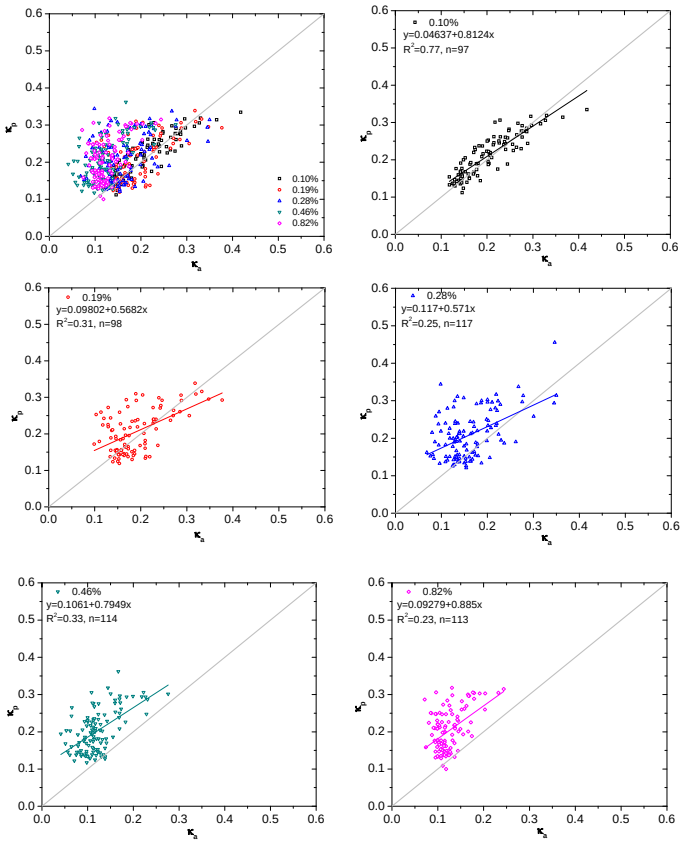

Fig. 15. Effective hygroscopicity parameters predicted from the sulfate and organic mass fractions determined by integral AMS measurements (κ_p) plotted against the values obtained from CCN measurements (κ_a) for all investigated supersaturations **(a)** and for individual supersaturations (**b–f**, S=0.10–0.82%). The colored lines are standard linear least-squares fits, and the grey lines indicate 1:1.

ACPD
9, 3811–3870, 2009